Nat. Hazards Earth Syst. Sci., 26, 1479–1513, 2026
https://doi.org/10.5194/nhess-26-1479-2026

Natural Hazards and Earth System Sciences
Open Access
EGU

What controls fire size in the South American Gran Chaco? Exploring atmospheric and landscape drivers through Remote Sensing

Rodrigo San Martín[1,♀], Catherine Ottlé[1], Anna Sörensson[2,3,4], Pradeebane Vaittinada Ayar[1], Florent Mouillot[5], and Marielle Malfante[6]

[1]Laboratoire des Sciences du Climat et de l'Environnement, LSCE/IPSL, CEA-CNRS-UVSQ, Université Paris-Saclay, Gif-sur-Yvette, France
[2]Centro de Investigaciones del Mar y la Atmósfera (CIMA), CONICET – Universidad de Buenos Aires, Buenos Aires, Argentina
[3]CNRS, CNRS – IRD – CONICET – UBA, Instituto Franco-Argentino para el Estudio del Clima y sus Impactos (IRL 3351 IFAECI), Buenos Aires, Argentina
[4]Facultad de Ciencias Exactas y Naturales, Universidad de Buenos Aires, Buenos Aires, Argentina
[5]UMR CEFE, University of Montpellier, CNRS, EPHE, IRD, Montpellier, France
[6]Univ. Grenoble Alpes, CEA, List, Grenoble, France
♀*Invited contribution by Rodrigo San Martín, recipient of the EGU Biogeosciences Outstanding Student and PhD candidate Presentation Award 2023.*

Correspondence: Rodrigo San Martín (rodrigo.sanmartin@lsce.ipsl.fr)

Received: 18 July 2025 – Discussion started: 11 August 2025
Revised: 12 December 2025 – Accepted: 26 February 2026 – Published: 24 March 2026

Abstract. Wildfires are key ecological agents in the Gran Chaco, one of the world's largest tropical dry forest systems. We analyzed more than 100 000 fire patches across the Wet, Dry and Very Dry Chaco between 2001 and 2022, to quantify environmental and anthropogenic controls on fire size. Fire sizes were strongly right-skewed: more than 80 % were smaller than 5 km^2, yet large and extreme fires dominated total burned area. Megafires (> 100 km^2) occurred in all subregions, while gigafires (> 1000 km^2) were rare but concentrated in the Dry Chaco. Fire Weather Index–burned area correlations exhibited strong spatial contrasts, reaching values of up to $r = 0.7$ in the Wet Chaco and showing weaker, more heterogeneous relationships in drier regions. Meteorological conditions during fires, particularly persistent strong winds, were associated with larger and more elongated patches. Random Forest models showed that topography and land cover composition together accounted for about 60 % of total SHAP importance, whereas demographic variables had very low SHAP contributions in the models. Human pressures shape ignition timing but showed limited direct influence on fire size once landscape structure was included in the models. These results provide a quantitative basis for improving regional fire danger assessments in the Gran Chaco.

1 Introduction

Wildfires shape global ecosystems by influencing vegetation structure, biodiversity, and landscape composition (Bowman et al., 2009; Archibald et al., 2013; Chuvieco et al., 2020). The Gran Chaco, spanning around 1.1 million km^2 across Argentina, Bolivia, Paraguay, and Brazil, is one of the largest remaining dry forest ecosystems, with marked variation in precipitation, vegetation, and human land use (Morello and Adámoli, 1968; Olson et al., 2001; Ginzburg et al., 2005; Torrella and Adámoli, 2005). Fire has long modulated its vegetation structure and driven transitions between forests, shrublands, and grasslands (Bucher, 1982; Kunst et al., 2003; Vidal-Riveros et al., 2023).

In recent decades, fire regimes in the Gran Chaco have shifted under the combined influence of land-use intensification, changes in fire use and suppression practices, and increasing climatic variability (Gasparri et al., 2008; De Marzo et al., 2021; Baumann et al., 2022; Marengo et al., 2022; Vidal-Riveros et al., 2023; San Martín et al., 2023; San Martín, 2024).

Fuel characteristics and availability play a central role (Bravo et al., 2014; Argañaraz et al., 2016, 2018; Vidal-Riveros et al., 2023). In native grasslands and savannas of the Gran Chaco, fine fuels typically reach 4000 to 5000 kg of dry biomass per hectare per year, supporting medium to high intensity surface fires (Bravo et al., 2025). In productive systems such as silvopastoral areas or improved pastures, implanted tropical forage grasses can increase fine-fuel loads substantially (up to double the biomass), locally enhancing fire intensity (Kunst et al., 2016).

Landscape heterogeneity further controls fire propagation, as the juxtaposition of rivers, wetlands, shrublands, forests and grasslands in the Gran Chaco, together with traditional firebreak construction and other local management practices, often restricts fire spread and creates natural or managed barriers to fire (Kunst et al., 2003; San Martín et al., 2023; Vidal-Riveros et al., 2023; Bravo et al., 2025). These interacting landscape controls challenge the idea of uniform and spatially consistent anthropogenic effects on fire regimes across global dry ecosystems (Bistinas et al., 2014; Andela et al., 2017; Archibald et al., 2018; Kelley et al., 2019; Jones et al., 2022).

Human activity is also a central component of fire regimes in the Gran Chaco. Across the region, most ignitions originate from rural land management practices, including pasture renewal burns, garbage burning, intentional clearing for agriculture or real-estate conversion, and opportunistic burning associated with hunting (Naval Fernández et al., 2023; Vidal-Riveros et al., 2023; San Martín et al., 2023; San Martín, 2024; Bravo et al., 2025). In the wetlands and floodplain grasslands of the Wet Chaco, intentional burning for pasture renovation or vegetation clearing typically occurs towards the end of winter and beginning of spring (end of the cold dry season) and, to a lesser extent, in late summer (towards the end of the wet season) (San Martín et al., 2023). Winter burns are usually controlled and produce small, patchy scars, whereas late-summer fires are more prone to escape and become larger, particularly in anomalous dry years (Saucedo and Kurtz, 2025). Despite these differences in fire behavior, vegetation often shows rapid post-fire recovery in the Wet Chaco (Bravo et al., 2025; Saucedo and Kurtz, 2025). In contrast, the central and western Dry Chaco show a higher prevalence of land-management fires linked to deforestation, rangeland conversion, and dry-season vegetation clearing (Baumann et al., 2022; Gasparri et al., 2008; Naval Fernández et al., 2023; San Martín et al., 2023). Between 2001 and 2019, nearly 40 % of the $\sim 51\,000\,km^2$ of deforested area in the Argentine Dry Chaco was associated with burned surfaces (San Martín et al., 2023).

Cultural dimensions further contribute to the heterogeneity of ignition contexts across the Gran Chaco. Fire use varies among actors, from small-scale subsistence cultivation in indigenous and rural communities to larger-scale land clearing by commercial producers and private ranchers (Vidal-Riveros et al., 2023). In parallel, indigenous wildfire narratives encode detailed ecological knowledge about fire causes, behavior and post-fire recovery (Sugiyama et al., 2025), underscoring that fire is embedded in diverse social and ecological understandings rather than representing a uniform anthropogenic pressure.

In this context, the 2020 fire season illustrated how socio-environmental factors interact under exceptional circumstances. The COVID-19 pandemic altered mobility, enforcement capacity and on-the-ground fire management across many regions worldwide. As discussed by Naval Fernández et al. (2023), in several fire-prone landscapes, such as the Brazilian Pantanal and other tropical savannas, the reduction or suspension of field surveillance and firefighting activities during lockdowns led to increased fire activity (Garcia et al., 2021; Kumar et al., 2022; Eklund et al., 2022). In contrast, in other regions, strict mobility restrictions reduced human-caused ignitions, highlighting the strong coupling between human presence and fire occurrence, as reported for regions in Asia and North America (Paudel, 2021; Poulter et al., 2021). In the Gran Chaco and adjacent drylands of central Argentina, mobility also declined sharply during the peak fire months, yet suppression capacity remained relatively stable due to the continued availability of volunteer brigades (Naval Fernández et al., 2023). Recent socio-anthropological work further shows that the lockdown period through 2020 overlapped with ongoing agrarian expansion and land-clearing dynamics, with deforestation, burning and road-infrastructure projects proceeding despite mobility restrictions, reinforcing long-standing territorial inequalities and weak institutional fire governance (Castilla, 2021; Schmidt and Castilla, 2023). This combination indicates that many ignitions were not accidental or urban in origin, but instead linked to rural land-clearing practices, pasture renewal and other management activities, underscoring the central role of human agency even under atypical social conditions (Naval Fernández et al., 2023; San Martín, 2024).

At broader temporal and spatial scales, climatic variability, especially the occurrence of prolonged droughts related to the intensification of episodes of multi-year strong El Niño–Southern Oscillation (ENSO) negative phases (La Niña), has been associated with large fire seasons in the Chaco and neighboring biomes (Alencar et al., 2015; Naumann et al., 2023). These climate anomalies reduce fuel moisture and extend the window for fire spread (Doblas-Reyes et al., 2021; De Marzo et al., 2023; Arias et al., 2024). In particular, several recent extreme fire seasons coincided with the 2020–2023 La Niña, which strongly affected moisture availability

and fire activity throughout the Gran Chaco and its surroundings (Kumar et al., 2022; Naval Fernández et al., 2023; San Martín, 2024).

Although individual drivers of fire occurrence are increasingly well understood, the way these factors interact to determine the final size of fires in the Gran Chaco remains poorly quantified. Existing studies highlight the importance of drought, fuel moisture deficits and human land use in shaping ignition patterns and BA totals, yet the mechanisms that control how far fires spread under contrasting environmental and land-use contexts remain unresolved (San Martín et al., 2023; Vidal-Riveros et al., 2023, 2024; Bravo et al., 2025). Baumann et al. (2022) showed that deforestation pathways vary by actor and context, altering fuel configurations and fire–landscape interactions, San Martín et al. (2023) demonstrated that precipitation–BA relationships differ markedly across land-cover types, and Levers et al. (2024) projected that continuing agribusiness expansion could intensify fire impacts on ecologically and socially sensitive areas. Together, these studies reveal substantial spatial heterogeneity in fire dynamics, but none explicitly evaluate how meteorological variability interacts with landscape structure and human pressures to shape final fire size.

Some classification efforts have begun to map regional fire diversity but still overlook key atmospheric determinants. Vidal-Riveros et al. (2024) grouped Paraguayan Chaco fire regimes by severity, frequency and extent, while Naval-Fernández et al. (2025) used multivariate clustering of landscape attributes to delineate pyroregions in the Argentine Chaco. These approaches captured meaningful spatial patterns, yet they did not incorporate high-resolution meteorological conditions, limiting their ability to identify the atmospheric processes that influence fire expansion.

In summary, no study has yet combined meteorological anomalies, fire morphology metrics, and landscape context to assess how short-term weather and long-term environmental gradients determine fire size in the Gran Chaco. This gap is critical given the biome's diverse ignition sources, propagation through heterogeneous fuels, and sharp transitions in hydrology, vegetation structure, and land-use intensity.

Advances in satellite Earth Observation now allow for such integration. Global burned area (BA) products such as FireCCI51 offer consistent daily burned surface estimates at moderate spatial resolution (Chuvieco et al., 2020). Event-based datasets including FRY (Laurent et al., 2018; Mouillot et al., 2023) and the Global Fire Atlas (Andela et al., 2019) reconstruct individual fires and enable the analysis of attributes such as ignition date, duration, size and morphology (Moreno et al., 2021; Takacs et al., 2021; García et al., 2022). In this study, we use FRYv2.0, which integrates the FRYv1.0 pixel aggregation method with the latest version of FireCCI51 BA mapping (Lizundia-Loiola et al., 2020), and we combine it with environmental and meteorological datasets to quantify how different drivers influence fire size across the Gran Chaco.

Specifically, we aim to answer the following scientific questions: (1) What are the primary fire-size characteristics and their frequency across the Gran Chaco between 2001 and 2022? (2) To what extent do meteorological conditions influence the size and expansion of individual fires? (3) Beyond weather, what roles do vegetation type, topography and human activity play in shaping fire size and fire occurrence across the region? (4) Which of these drivers best explain the spatial and temporal variability of fire size among the different subregions of the Gran Chaco?

2 Methods

2.1 Study area

The Gran Chaco is an extensive tropical and subtropical region of South America, covering approximately 1 100 000 km^2 (Fig. 1). It contains the world's largest continuous dry tropical forest and extensive wetland systems (Bucher, 1982; Olson et al., 2001). In the literature, terminology varies with references to the South American Chaco, the Gran Chaco, or just Chaco. To avoid confusion, we only use Gran Chaco in this work.

The region is mostly flat and low (< 200 m), with higher and undulating terrain towards the northeast limit (up to ~ 500 m), the western Andean foothills (up to ~ 2000 m), and the southwestern Sierras de Córdoba (reaching 2790 m at Mt. Champaquí). Following Olson et al. (2001), we delimit a humid eastern Wet Chaco from a drier western Dry Chaco, structured along marked west–east gradients in precipitation, vegetation, and hydrology (Morello and Adámoli, 1968; Bucher, 1982; Ginzburg et al., 2005; Torrella and Adámoli, 2005). Following Baumann et al. (2018), we further identify a drier southwestern subregion referred to as the Very Dry Chaco, characterized by lower biomass, greater aridity, higher elevations, and distinct fire regimes. Its extent is delimited by the Argentine provincial borders of Mendoza, San Luis, Córdoba, San Juan, and La Rioja.

For the 2001–2020 period, mean annual precipitation averaged approximately 600 mm yr^{-1} in the Very Dry Chaco, 860 mm yr^{-1} in the Dry Chaco, and 1375 mm yr^{-1} in the Wet Chaco, with local maxima in the eastern sector approaching 1800 mm yr^{-1} (San Martín et al., 2023; San Martín, 2024). These precipitation differences are reflected in contrasting land-cover structures: the Wet Chaco includes extensive wetlands, floodplains, grasslands, and palm savannas; the Dry Chaco is dominated by drought-adapted forests and shrublands increasingly interspersed with agricultural fields; and the Very Dry Chaco is characterized by more open shrublands and dry forest patches.

Regarding its hydrology, the Gran Chaco forms part of the La Plata basin (Barros et al., 2006; Musser, 2010). Rivers such as the Pilcomayo, Bermejo, and Salado originate in the Andes, cross the Dry Chaco, and disperse into alluvial

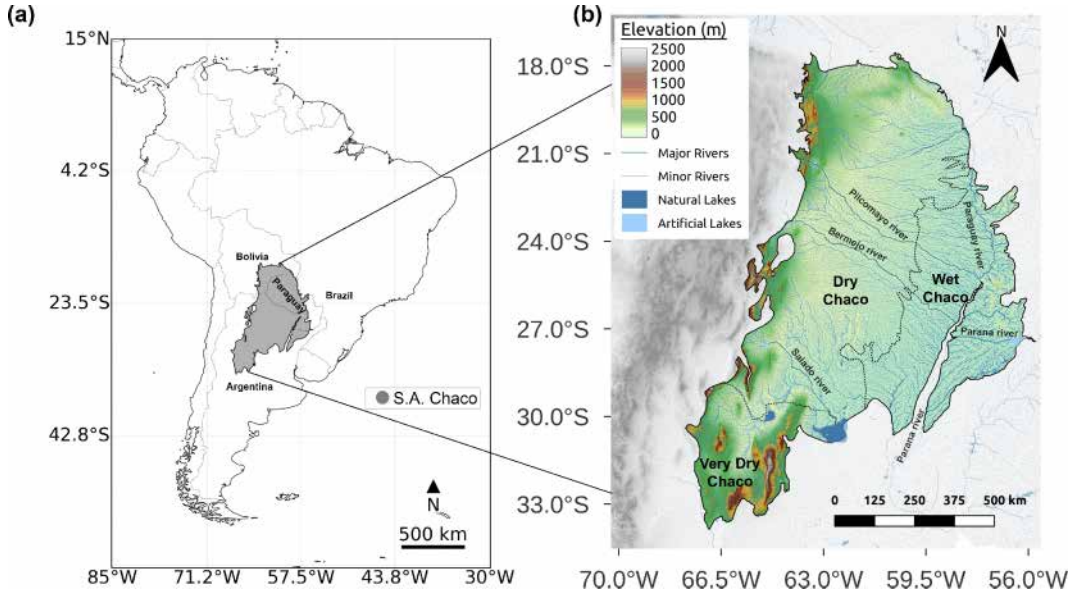

Figure 1. The Gran Chaco location in South America **(a)** and its topography **(b)** with its different subregions, main rivers, and lakes. Based on Shuttle Radar Topography Mission (SRTM) at 90 m (SRTM | NASA Earthdata, 2024) and HydroSHEDS (Lehner et al., 2008).

megafans, streams, and wetlands in the eastern Wet Chaco. This west–east hydrological gradient drives seasonal contrasts: in dry months, the Dry Chaco faces water scarcity, whereas the Wet Chaco retains permanent wetlands that sustain ecological processes and fauna (Cabrera, 1976; Bucher, 1982; San Martín, 2024). Additionally, the region harbors exceptional biodiversity, with over 3400 plant species and hundreds of vertebrates, many endemic (Redford et al., 1990; Bucher and Huszar, 1999; Nori et al., 2016).

Fire activity shows pronounced subregional contrasts across the Gran Chaco. The Wet Chaco presents a bimodal fire season, with peaks at the end of the warm wet season (late summer–autumn) and again at the end of the cold dry season (late winter–spring), while the Dry Chaco exhibits a unimodal pattern restricted to the end of the cold dry season, towards late winter–spring (Kunst and Bravo, 2003; Bravo et al., 2010, 2025; San Martín et al., 2023). Mean annual BA is about 15 000 $km^2\ yr^{-1}$ in the Wet Chaco and roughly 8500 $km^2\ yr^{-1}$ in the Dry and Very Dry Chaco together, based on annual BA totals for 2001–2019. Despite its higher annual BA, much of the Wet Chaco burns repeatedly, with ∼ 57 % of its burned surface experiencing at least two fire events between 2001 and 2019. In contrast, about 66 % of the burned surface in the Dry Chaco represents one-time fires, with burns advancing over previously unburned forests. In this western subregion, fires typically follow deforestation rather than acting as the primary clearing mechanism (San Martín et al., 2023). These contrasts reflect the greater continuity of fine fuels and higher fire recurrence in the eastern Wet Chaco, compared with the more intermittent and fuel limited conditions characterizing the Dry and Very Dry Chaco.

2.2 Datasets

2.2.1 Fire patches

In this study, we used FRYv2.0, a recent global database of fire patch (FP) functional traits (morphology, fire spread, and timing) to investigate fire dynamics and their underlying drivers in the Gran Chaco (Laurent et al., 2018; Mouillot et al., 2023). FRYv2.0 is an updated, second-generation version of the original FRY database that aggregates burned area (BA) pixels from the latest FireCCI51 dataset and from the MODIS MCD64A1 product into individual FPs using fixed temporal cut-offs of 6, 12, or 24 d to delimit the extent of a fire event or the onset of a new one. Compared with the original release, it provides extended patch-level information, including morphology (for example area, perimeter, shape index, core area), temporal traits such as burn dates and duration, dynamic traits such as rate of spread, fire radiative power (FRP) and severity indicators, and associated land cover. The FRYv2.0 morphological metrics describe the geometry and structure of each FP: *n_cell* quantifies the number of burned pixels from the input BA product that form the fire patch; area represents the total burned surface; the *shape index* captures deviations from a compact circular shape; the *core-area index* indicates the proportion of interior, non-edge area; *eccentricity* measures patch elongation; and the *perimeter-to-area ratio* characterizes boundary complexity and compactness.

Patch-level functional traits are computed only for patches composed of at least five burned pixels, to avoid geometric and orientational instability in very small patches. FRP-based diagnostics, including ignition timing derived from active-fire detections, are assigned only to patches larger than 100 ha (approximately sixteen FireCCI51 pixels). This ignition dating offers a more accurate estimate of fire onset than the default burn-date information in FireCCI51 or MODIS MCD64A1, which relies on the day of first BA detection.

For this work, we selected the FRYv2.0 version based on FireCCI51 rather than the version based on the MODIS MCD64A1 BA product, because the FireCCI51 input has higher spatial resolution (250 m compared to 500 m), provides better spatial detail for the heterogeneous landscapes of the Gran Chaco, and ensures consistency with our previous FireCCI51 based analysis (San Martín et al., 2023), thus avoiding additional uncertainty from mixing BA products. The FRYv2.0 FireCCI51-based dataset used here is publicly available at https://osf.io/rjvz5/files/osfstorage (last access: 10 June 2025).

2.2.2 Meteorological Data

To study meteorological and climate time series in the region, we used the ERA5-Land global reanalysis dataset focused on land surface variables, developed by the European Centre for Medium-Range Weather Forecasts (ECMWF) (Muñoz-Sabater et al., 2021). It provides high-resolution data for land–atmosphere interactions, designed to improve the ERA5 dataset by offering finer detail (0.1° instead of 0.25° spatial resolution) for variables affecting the land surface.

The product is available in the Copernicus Data Store (CDS) in NetCDF at https://cds.climate.copernicus.eu/cdsapp#!/dataset/reanalysis-era5-land (last access: 30 May 2024). We downloaded hourly data arrays covering January 2001 through January 2023.

2.2.3 Environmental and Anthropogenic Data

We compiled several spatial datasets that represent biophysical conditions and human-related drivers relevant to fire activity in the Gran Chaco.

Topography was obtained from the NASA SRTM v3 product (https://srtm.csi.cgiar.org, last access: 26 May 2025). This product provides a 3 arcsec (approximately 90 m) digital elevation model (DEM) in WGS84 geographic coordinates. Slope and aspect were calculated from this DEM using the Horn algorithm as implemented in the richdem TerrainAttribute function, which estimates local gradients over 3 by 3 cells (Horn, 1981).

Land cover (LC) was obtained from the ESA Climate Change Initiative Moderate Resolution Land Cover product (CCI MRLC; https://cds.climate.copernicus.eu/datasets/satellite-land-cover, last access: 26 May 2025). This product provides annual maps at 300 m spatial resolution for the period 1992 to 2022. We selected CCI MRLC because its resolution is appropriate for the regional extent of this study, which covers more than 1 100 000 km^2. The product has undergone extensive validation, is widely used in regional land surface studies, and ensures consistency with our previous analyses in the Gran Chaco (Defourny et al., 2023; Harper et al., 2023; San Martín et al., 2023).

Fuel accumulation before each fire was characterized using MODIS LAI at 500 m resolution and 8 d intervals. We used MOD15A2H (Terra) for 2001 to 2002 and MCD15A2H (Terra and Aqua combined) for 2002 to 2023. Only observations with quality level 0 were retained. For each fire, we extracted all LAI values from MODIS pixels that overlapped the fire patch. To represent the accumulated biomass that could contribute to fire spread, we defined the pre-fire period as the interval between 1 August of the year before the fire and the ignition date. This window captures the seasonal minimum at the end of the winter dry season and the entire subsequent growing season. A 4-step rolling mean with a minimum of one valid value was applied to reduce high frequency noise. The final pre-fire LAI value for each fire patch was the mean LAI across this August to ignition interval. This variable, which we refer to as the mean LAI of the previous growing season, served as a proxy for the biomass accumulated before the fire.

Soil properties were obtained from the SoilGrids250m database. The variables used were soil organic carbon at 0 to 5 cm depth, sand fraction, and bulk density. We used the one-kilometer aggregated layers provided by SoilGrids and computed means for each fire patch.

Population density was taken from the Gridded Population of the World version 4 (GPWv4) (CIESIN, 2017; https://www.earthdata.nasa.gov/data/projects/gpw, last access: 25 November 2025). The native resolution of this product is approximately 30 km. Since the dataset was not modified, population values were assigned to each fire patch using nearest neighbor extraction.

Livestock density was obtained from the Gridded Livestock of the World version 4 (GLWv4; https://dataverse.harvard.edu/dataverse/glw_4, last access: 25 November 2025). This dataset is available at roughly 10 km resolution. The original values were used as provided. For each fire patch, livestock density (number of cattle per km^2) was summarized using zonal means.

Road density was derived from two global road network datasets to account for uncertainties in road mapping, particularly the incomplete representation of informal, unpaved or irregular roads in some regions of the Gran Chaco. We used two independent sources: OpenStreetMap (OSM; https://www.openstreetmap.org, last access: 25 November 2025), which is community-curated and generally more complete in populated areas, and the Microsoft Bing AI Global Roads dataset (MS; https://github.com/microsoft/RoadDetections, last access: 25 November 2025), which is algorithmically extracted from high-resolution satellite imagery and tends

to provide broader coverage in rural and sparsely populated landscapes. For all main analyses, road density was computed from the OSM dataset, while the MS product was used only in a sensitivity experiment to evaluate the robustness of road-related effects (see Sect. 2.3.9).

Roads were maintained in vector format and intersected with a regular 0.03° grid (∼ 3 km), projected onto an equal-area coordinate system for accurate calculations of road length and cell area. Road density (km km^{-2}) was computed for each grid cell, and fire patches were assigned an area-weighted mean value based on all overlapping cells. The 0.03° resolution was selected after testing coarser and finer grids, providing the best trade-off between capturing road density within each patch and preserving the surrounding spatial context while maintaining consistency across both road datasets. Using both products in this way ensured that the inferred influence of human accessibility on fire behavior was not dependent on a single mapping dataset, while keeping OSM as the reference road layer for the core RF configurations.

2.2.4 Climate Oscillations

To account for the influence of large-scale climate variability, we included the Multivariate El Niño–Southern Oscillation (ENSO) Index version 2 (MEI.v2), developed by NOAA's Physical Sciences Laboratory. The MEI.v2 time series was obtained from NOAA PSL at https://psl.noaa.gov/enso/mei/ (last access: 26 May 2025).

2.3 Data processing and analysis methods

2.3.1 Fire Weather Index (FWI)

We built an ERA5-Land-based Canadian Fire Weather Index (FWI; Van Wagner, 1987) dataset for the Gran Chaco at 0.1° resolution and daily time steps. We converted hourly accumulated precipitation to hourly rainfall by differencing successive steps and summing totals from 15:00 UTC (day $D-1$) to 15:00 UTC (day D), matching the FWI daily window and corresponding to local noon in most of the Gran Chaco. We applied this fixed 15:00 UTC cutoff to the full region to avoid inconsistencies caused by varying national time zones and daylight-saving changes.

We extracted daily meteorological inputs (i.e., air temperature, relative humidity, wind speed at local noon, and 24 h precipitation) to compute the six FWI sub-indices: Fine Fuel Moisture Code (FFMC), Duff Moisture Code (DMC), Drought Code (DC), Initial Spread Index (ISI), Build-Up Index (BUI), and FWI. We performed calculations with an adapted version of the FireDanger Python package (https://github.com/steidani/FireDanger, last access: 25 November 2025) compatible with xarray and NetCDF, including pixel-level day length for DMC and hemisphere-specific drying factors for DC. We initialized the system on 1 January 1981 using Copernicus ERA5–FWI moisture codes at 0.25° (Vitolo et al., 2020) interpolated to 0.1°.

2.3.2 Land Cover processing

For this work, the original classes of CCI MRLC were grouped into eight categories relevant to the Gran Chaco fire regime. These categories included tree cover, shrublands, grasslands, seasonally flooded herbaceous vegetation, croplands, two mixed mosaics containing combinations of herbaceous and woody vegetation, and an extra class we called "Others", grouping the remaining underrepresented classes in the Gran Chaco. For each FP we extracted the fractions of LC at the year of fire ignition, and these fractions were used to calculate the following landscape heterogeneity indices:

In order to quantify the landscape heterogeneity within each FP and assess how the mix and spatial balance of LC types influence fire outcomes, we calculated the Shannon diversity index (H) and Pielou's evenness (E). They were computed as follows:

Shannon Diversity Index (Shannon, 1948):

$$H = -\sum_{i=1}^{m} p_i \log(\mathrm{p}_i) \tag{1}$$

where m is the number of land cover classes present in the fire patch, p_i is the proportion of land cover type i, and the sum includes all classes with $p_i > 0$.

Pielou's evenness (Pielou, 1966):

$$E = \frac{H}{\log(m)} \tag{2}$$

where H is the Shannon Diversity Index and m is the number of land cover classes present in the fire patch.

2.3.3 Wind indices

Using ERA5-Land data, we calculated for each FP a metric specifically designed to capture the role of strong, persistent winds in shaping fire behavior: the Extreme Wind and Direction Index (EW_dir_index). This index measures both how often extreme winds occurred and how steady their direction was.

The first component, fraction of extreme-wind days (EW_frac), is the proportion of burning days when the daily maximum wind speed exceeded 25 km h^{-1}:

Extreme Wind Days Fraction:

$$\mathrm{EW\_frac} = \frac{\mathrm{EW}}{N} \tag{3}$$

where EW is the number of days with extreme winds and N is the total fire duration (days). High values indicate that strong winds occurred on many burning days.

The second component, wind direction steadiness (wind_dir_R), reflects how consistent the wind direction

was across the fire's duration (N). Each day's mean wind direction (θ_i, in radians) is represented as a unit vector, summed across all days, and normalized by the fire duration:

Wind Directionality Index:

$$\text{wind\_dir\_R} = \frac{\sqrt{\left(\sum_{i=1}^{N}\cos\theta_i\right)^2 + \left(\sum_{i=1}^{N}\sin\theta_i\right)^2}}{N} \quad (4)$$

Values near 1 mean that winds blew in a stable direction throughout the event, while values near 0 mean that wind directions shifted substantially from day to day.

The EW_dir_index is the product of EW_frac and wind_dir_R:

Extreme Wind and Direction Index:

$$\text{EW\_dir\_index} = \text{EW\_frac} \times \text{wind\_dir\_R} \quad (5)$$

It reaches high values only when strong winds occur on many burning days and blow consistently from the same direction, identifying fires likely driven by sustained, unidirectional wind conditions.

2.3.4 Burned Area vs Fire Counts

To examine the interannual relationship between fire counts and total BA, we compared annual BA and annual fire counts for each of the three Gran Chaco subregions using FRYv2.0. For every year in 2001–2022, total BA was computed as the sum of the burned surface of all fire patches within each subregion, while fire counts were obtained as the number of individual patches whose ignition date fell within that year. We then fitted simple linear regressions between annual BA and annual fire counts for each subregion to quantify how ignition frequency explains interannual variability in BA and to assess whether this relationship differs among the subregions and between the wet and dry seasons.

2.3.5 Fire size classification

To examine how fires of different magnitudes contribute to overall fire activity in the Gran Chaco, we classified all FRYv2.0 fire patches (FPs) into six size categories. Fire events can be grouped according to various criteria, including behavior (e.g., rate of spread, intensity), ecological impact (e.g., severity), structural properties (e.g., shape, perimeter), or final extent (total burned area). Because our objective is to identify the determinants of final fire size, we adopted a size-based classification. This approach directly aligns the categorization with the response variable and facilitates interpretation of the climatic, landscape, and anthropogenic drivers controlling it.

To avoid ad-hoc or region-specific thresholds, we followed the standardized fire-size typology proposed by Linley et al. (2022), who conducted the first global assessment aimed at harmonizing terminology for large fires. They argue that terms such as "megafire" or "large wildfire" had been used inconsistently across disciplines and agencies, often referring to different orders of magnitude depending on national contexts or management traditions. They show that this lack of standardization complicates cross-regional comparison and the interpretation of extreme events. To resolve this, they propose clear, size-based definitions applicable worldwide: megafires as events with BA $>$ 10 000 ha (100 km^2), gigafires $>$ 100 000 ha (1000 km^2), and terafires $>$ 1 000 000 ha (10 000 km^2). Their framework is explicitly designed for satellite-derived BA products, including those used to build FRY, and provides a consistent basis for global and regional analyses.

Using Linley's typology ensures that extreme fire classes in the Gran Chaco are comparable to global assessments and avoids relying on operational thresholds used in some countries (e.g., 40 000 ha) that lack a physical or ecological rationale. At the same time, the empirical distribution of FRYv2.0 patch sizes in the Chaco is strongly right-skewed, with most events being small and only a few exceeding the megafire threshold. For this reason, and to retain regional relevance, we added to Linley's standardized thresholds four smaller size classes suitable for the Gran Chaco, while preserving the key cut-offs at 100 and 1000 km^2. FRYv2.0 imposes a practical lower limit on measurable patch size: functional traits are computed only for patches composed of at least five FireCCI51 pixels ($\sim$ 0.3 km^2), and FRP-based diagnostics, including ignition dating, are provided only for patches larger than $\sim$ 100 ha (1 km^2; see Sect. 2.2.1). This naturally defines the smallest reliable category in our system.

The resulting scheme spans from a "very small" class (0–1 km^2), which is more uncertain because FRY patches in this range often lack complete geometric or FRP-based diagnostics, through small (1–5 km^2), medium (5–10 km^2), and large (10–100 km^2) events, up to megafires (100–1000 km^2) and gigafires ($>$ 1000 km^2). No fire in the Gran Chaco exceeded 10 000 km^2, and therefore the terafire class defined by Linley et al. (2022) is not used in this work.

2.3.6 Gridded burned area

To enable a spatiotemporal comparison between fire activity from FRYv2.0 fire patches and meteorology, we developed a pipeline to transform the FP-based data into a monthly gridded product at 0.1°, matching the ERA5-Land grid (Fig. 2).

The temporal assignment of fires to months followed a hybrid strategy: where MODIS-derived hotspot detection dates (mindtc_frp and maxdtc_frp) were available in a given FP (typically absent in very small FPs) they were used. Both FireCCI51- and MODIS-based versions of FRYv2.0 include these hotspot date variables when available for the FP. When hotspot dates were missing, we used the FireCCI51-derived burn dates (minBD and maxBD), which are based on surface reflectance changes and are available for all FPs. For FPs spanning multiple months, we assigned the fire to the month in which it started, unless its duration in a subsequent

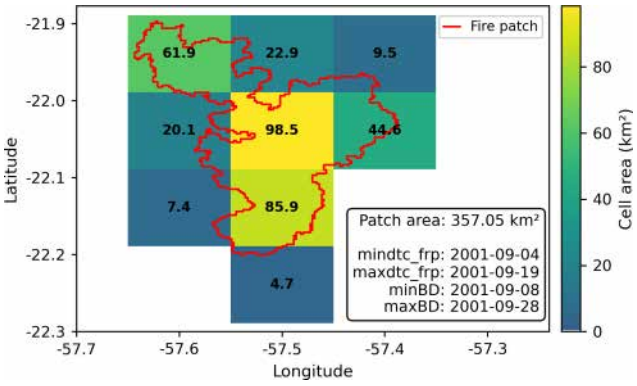

Figure 2. Example of one FRY fire patch (red line) over the gridded FRY dataset. Each grid cell at 0.1° is assigned the burned area corresponding to the total fraction of the patch that overlaps it. The values printed over each grid cell correspond to these values.

month exceeded that of the starting month by more than two days.

Each FP was rasterized on a 0.01° grid by intersecting it with individual cells. The intersected area in square kilometers was computed using the WGS84 ellipsoid model. These contributions were aggregated per cell and per assigned month to build a three-dimensional array of monthly BA (lat × lon × time). A similar procedure was implemented for fire counts, using ignition (first detection) coordinates and dates. Each FP's fire ignition coordinate was allocated to the closest cell in the 0.1° grid. The resulting monthly gridded dataset included two variables: BA and counts.

2.3.7 Anomalies and climatologies

For all ERA5-Land variables, as well as the FWI index and its sub-indices, we computed pixel-level daily climatologies using the 2001–2020 mean as the baseline. Meteorological anomalies were then defined as the daily deviation from this climatology and subsequently aggregated to monthly values to match the temporal scale of the BA analysis.

To compute monthly BA anomalies, we derived pixel-level monthly climatologies for the period 2001–2020 from the gridded BA dataset. Anomalies were defined as the difference between each monthly BA value and the corresponding monthly climatological mean, following the same temporal normalization applied to meteorological variables. This anomaly-based formulation was used only for the correlation analysis with FWI anomalies and not for any other statistical or spatial analyses in the manuscript.

For the specific analysis comparing monthly BA anomalies with monthly FWI anomalies, only pixels with at least four fire-active months (BA > 0) during 2001–2022 were retained to avoid artefacts from sparsely populated or highly skewed anomaly series. Correlations were computed using both Pearson's coefficient and Spearman's rank coefficient.

We did not apply an FWI95-based threshold or similar fixed-percentile metrics, as these are less comparable across the strong climatic gradient of the Gran Chaco and may artificially amplify or dampen fire–weather relationships depending on local baseline conditions. Using pixel-level anomalies instead allows each location to be evaluated relative to its own climatology, yielding a spatially consistent and locally meaningful basis for comparison.

2.3.8 Fire-weather types

We classified fire patches (FPs) into three groups based on associated atmospheric conditions using the K-means clustering algorithm (MacQueen, 1967) in Python's scikit-learn v1.3. This approach follows prior applications in fire studies (Ruffault et al., 2016, 2020; Vidal-Riveros et al., 2024) and aimed to identify distinct fire-weather types (FWTs) and assess their influence on fire size and shape.

For this clustering analysis, we retained only fire patches between 1 and 100 km^2 ($N = 78\,052$). At the lower end, this choice is consistent with the construction of the FRYv2.0 database, where the FP functional traits are computed only for patches composed of at least five burned pixels and smaller patches are filtered out because their geometry and orientation are considered unreliable (see Sect. 2.2.1). In addition, FRP based diagnostics, including ignition timing derived from active fire detections, are only provided for FPs larger than 1 km^2 (approximately 16 FireCCI51 pixels), so the smallest events lack both robust geometric traits and FRP timing information. At the upper end, fires larger than 100 km^2 were excluded from the K-means analysis. In addition to their low frequency, these very large, long duration patches often span heterogeneous landscapes and experience several distinct weather situations over their burning period, so the associated ERA5-Land and FWI time series mix conditions from distant locations and different days. This mixing makes the patch-averaged meteorological descriptors difficult to interpret as a single coherent FWT and would likely introduce substantial biases in the clustering and in the Random Forest (RF) models used later to analyze fire size drivers (see Sect. 2.3.9).

For each FP within the 1–100 km^2 range, we extracted daily ERA5-Land meteorological data and the computed FWI time series from 7 months before ignition to 7 months after, and then built two feature sets, one representing pre-fire conditions and one representing conditions during the fire.

For the Pre-Fire set, we used normalized anomalies of 2 m air temperature, 10 m wind speed, relative humidity (RH), drought code (DC), and duff moisture code (DMC) (Ruffault et al., 2020). Pre-fire values were calculated as the 3 d mean from ignition day (D) to $D - 2$ to limit detection-date bias (Lizundia-Loiola et al., 2020; Pettinari et al., 2021) while avoiding noise from longer lags.

For the During-Fire set, we computed the same variables averaged over the fire's duration and added the Extreme

Wind Days Fraction and the Extreme Wind and Direction Index, described in Sect. 2.3.3.

All variables in both sets were standardized before clustering (mean $= 0$, $\sigma = 1$). The resulting data matrix was clustered with $k = 3$, squared Euclidean distance, k-means++ initialization, 50 random restarts, and a convergence tolerance of 10^{-4}. We retained three clusters based on a prior hypothesis (wind-driven, drought-driven, and neutral), an elbow in the within-cluster sum-of-squares curve, and a peak in the silhouette coefficient at $k = 3$.

Cluster labels were assigned by interpreting centroid positions in principal component space and examining the temporal evolution of variables (Fig. S1 in the Supplement). Robustness was assessed using mean silhouette coefficients and their distribution across clusters. The first two principal components explained more than 60 % of the variance and clearly separated cluster centroids.

2.3.9 Fire size drivers

To investigate the role of environmental and anthropogenic variables in determining fire size, we extracted a diverse set of FP-level potential predictors encompassing topographic, climatic, anthropogenic, vegetation, and landscape heterogeneity dimensions. These variables, listed in Table 1, were used as inputs in the RF models to assess their relative importance in explaining fire size.

Once all potential predictor variables were derived, we trained RF models using a set of 17 explanatory variables to analyze the drivers of fire behavior, using the variable *n_cell* from the FRY dataset as the response variable. This variable represents the number of FireCCI51 pixels within each FP and was preferred over patch-based area due to the latter's dependency on latitude, which introduced artificial discontinuities. In contrast, *n_cell* provided a discrete and spatially consistent proxy for BA, improving model stability and interpretability.

We implemented 12 primary RF models across five configurations: (i) a global model using all the 78 052 fire patches used for the clustering analysis (patches with area between 1 and 100 km^2), (ii) three subregion-specific models for the Wet, Dry, and Very Dry Chaco, (iii) two seasonal models based on ignition season (wet vs dry), and (iv) two sets of three cluster-based models (pre-fire and during-fire conditions) derived from the FWT classification (see Sect. 2.3.8).

All models were trained using the ranger R package (Wright and Ziegler, 2017) with quantile regression forests (Meinshausen, 2006). We used 500 trees, a minimum node size of 5, variance-based importance, and the Poisson split rule, with 4 variables considered at each split. Feature selection included correlation filtering ($r > 0.8$ threshold) and preliminary importance scores. Each model was trained on 75 % of the data and validated on the remaining 25 %. We evaluated feature contributions using SHAP (SHapley Additive exPlanations) values.

In addition to these primary configurations, we trained two diagnostic RF models to assess the robustness of our results. First, a "No Topography" model was built by removing elevation and slope from the predictor set while keeping all other variables and settings identical to the Full Chaco configuration. Second, an "MS Roads" model replaced the OSM-based road-density layer with the MS-based road density, again using the same sample of fire patches, hyperparameters, and training/test split as the Full Chaco RF. These sensitivity experiments were analyzed with the same SHAP-based diagnostics as the primary models and were used to evaluate whether the RF results were robust to changes in the predictor set and road-data source.

3 Results

3.1 Burned area and ignitions

We examined the interannual variability of burned area (BA), fire counts, and mean fire duration across the Gran Chaco between 2001 and 2022 (Figs. 3; S3). To complement these indicators, we quantified the relationship between total BA and annual fire counts for each subregion and season, using linear correlations (Fig. S2).

The time series reveals a sustained decrease in annual fire counts and BA from the early 2000s to the late 2010s, followed by a pronounced peak in 2020–2021. Because the observational window begins in 2001, it is difficult to determine whether the downward phase reflects a longer-term trend or a segment of decadal variability. These two peak years also show the largest BA of the record, particularly in the Wet and Dry Chaco, and stand out clearly relative to the preceding trajectory.

BA and fire counts showed a broadly positive relationship, but with substantial regional and seasonal differences. In the Wet Chaco, BA and fire counts were strongly correlated in both wet and dry seasons ($R^2 = 0.96$ and 0.91; Fig. S2), indicating that interannual BA variability is largely explained by the annual number of fire patches rather than by individual fire sizes. Mean fire duration remained stable (approximately 10–12 d; Fig. S3).

The Dry Chaco exhibited a high wet-season correlation between BA and fire counts ($R^2 = 0.87$; Fig. S2), but a much weaker dry-season relationship ($R^2 = 0.45$). This implies that, during the dry season, fluctuations in BA are not tightly linked to fire counts, consistent with a larger contribution of size extremes. Fire duration was also stable through the period (Fig. S3).

Table 1. Target and potential predictor features extracted from each FRY fire patch within the Gran Chaco region, grouped by variable types. These features were used for the Random Forest models trained in this work.

Category	Variables
Fire Size (target feature)	Number of pixels within the fire patch (250 m pixels from FireCCI51)
Topography	Mean Slope (%) Mean Elevation (m)
Meteorology (during fire mean)	Precipitation (mm) Maximum Wind Speed (km h^{-1}) Extreme Wind and Direction Index (EW_dir_index) Extreme Wind Days Fraction (EW_frac)
Anthropogenic proxies (year of fire ignition)	Cattle Density (heads per km^2) Road Density (km km^{-2}) Population Density (p per km^2)
Vegetation productivity (previous growing season)	LAI for previous growing season (MODIS-derived)
Land Cover Composition (year of fire ignition)	Flooded Herbaceous vegetation (%) Tree Cover (%) Shrublands (%) Trees/Shrubs/Herbs Mosaics (%) Natural/Croplands Herbaceous Mosaics (%)
Landscape Heterogeneity (year of fire ignition)	Land Cover Diversity (Shannon Index, H) Land Cover Evenness (Pielou Index, E)

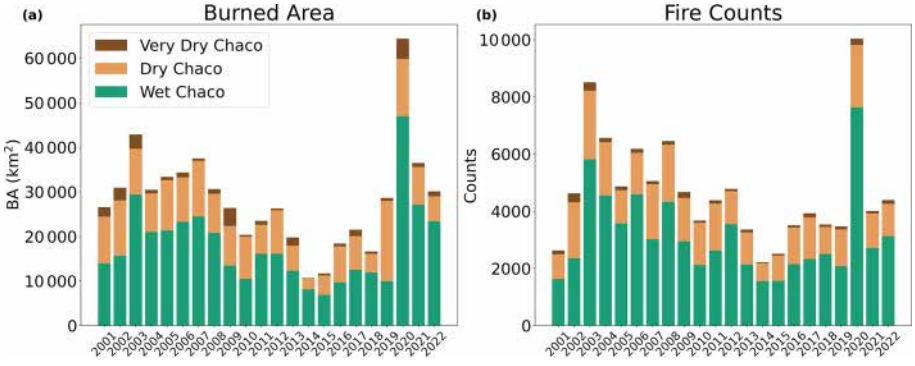

Figure 3. Interannual evolution of fire activity in the Gran Chaco from 2001 to 2022, derived from FRYv2.0 fire patches. **(a)** Total annual burned area and **(b)** total annual fire counts, with stacked bars showing the contributions of the Wet, Dry, and Very Dry Chaco subregions.

In the Very Dry Chaco, wet-season fires were infrequent and showed almost no relationship between BA and fire counts ($R^2 = 0.11$; Fig. S2). In contrast, dry-season BA correlated strongly with the number of fires ($R^2 = 0.78$). Mean fire duration was relatively constant, with no clear interannual trend (Fig. S3).

Overall, fire duration exhibited limited variation across subregions (Fig. S3), reinforcing that BA fluctuations were controlled primarily by changes in fire counts and the distribution of fire sizes, rather than by changes in the duration of individual fires.

3.2 Land Cover and Fire size distribution

Figure 4 shows land-cover (LC) distribution in 2001 and 2022 together with the spatial distribution of fire events, classified by size, between those years. Marked LC transitions occurred over the study period (Fig. 5), with substantial expansion of shrublands and mosaic vegetation and a net reduction of tree cover across the Chaco. Much of the increase in shrublands and mixed vegetation mosaics originates from former tree-cover classes (Fig. 5), indicating widespread forest degradation and structural simplification of vegetation that modifies fuel continuity.

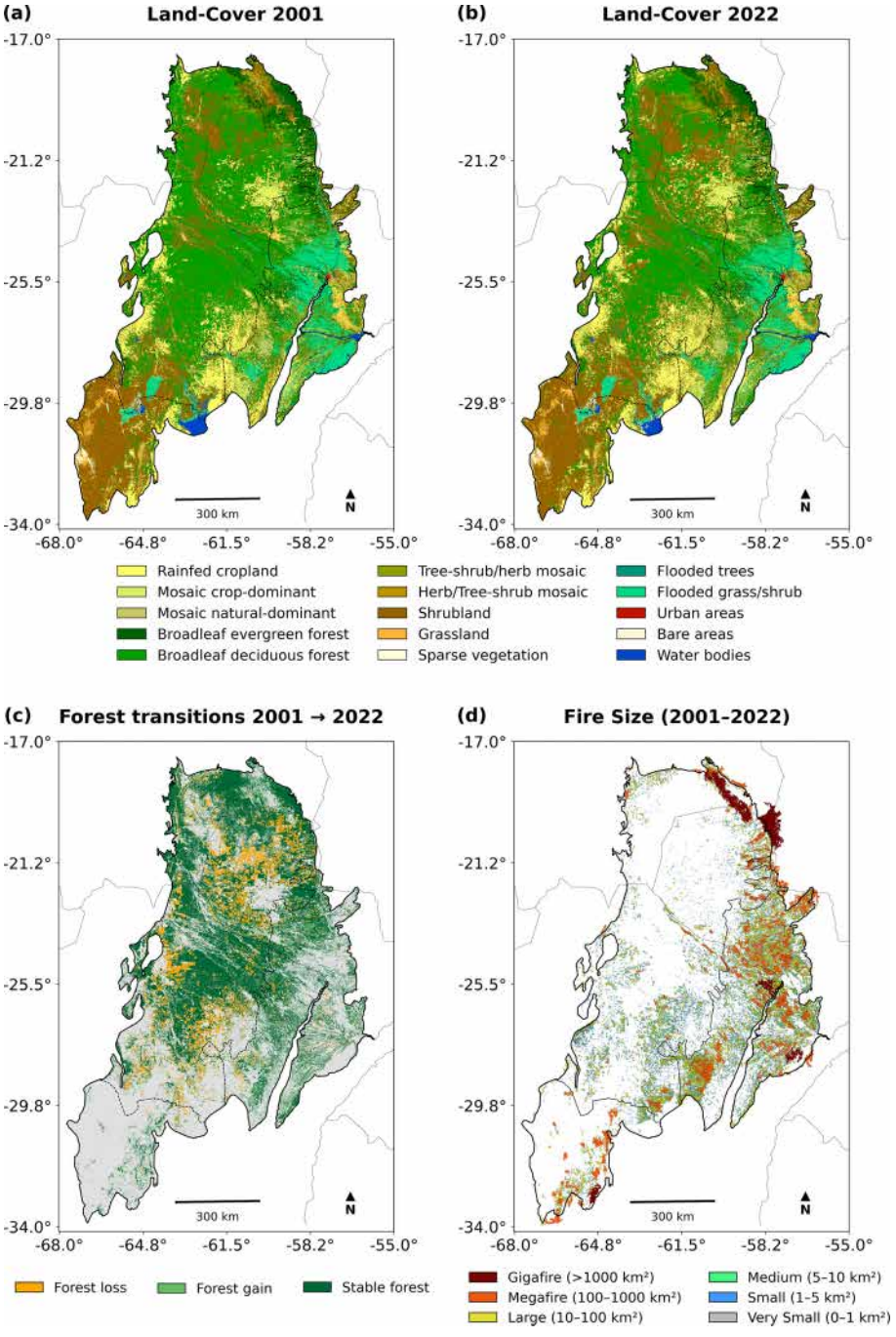

Figure 4. (a, b) Land-cover distribution in the Gran Chaco based on ESA-CCI MRLC for 2001 and 2022, respectively. **(c)** Forest transition classes between 2001 and 2022, showing forest loss (forest to non-forest), forest gain (non-forest to forest), and stable forest. Forests include all tree cover classes (shrubs not included); non-forest pixels appear in grey. **(d)** Spatial distribution of fire events (2001–2022) categorized by fire size using FRYv2.0 data. Fire-size classes range from Very Small ($< 1\,km^2$) to Gigafires ($> 1000\,km^2$). Fires patches overlapping the Chaco boundary are retained.

Across the full Gran Chaco, BA is dominated by open formations (Fig. S4): seasonally flooded grasses and herbs account for $\sim 26\,\%$ of total BA, shrublands for $\sim 23\,\%$, and mosaic vegetation for $\sim 12\,\%$. Tree-cover classes represent $\sim 24\,\%$ of total BA. Although forests are typically considered less flammable than floodplain grasses and shrublands, the proportion of BA affecting tree cover is comparable to that of these open formations, indicating that fires extensively affect forested and transitional landscapes.

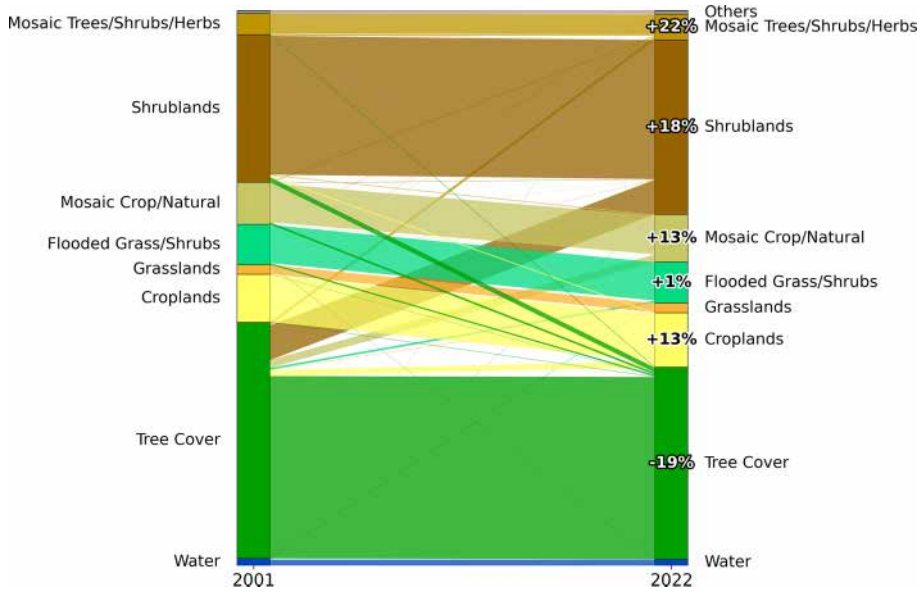

Figure 5. Sankey diagrams showing land-cover (LC) transitions between 2001 and 2022 across the Gran Chaco. LC classes were derived from the ESA CCI Medium Resolution Land Cover product and aggregated into the main classes present in the region. Percentages indicate the relative increase or decrease of each class between the two years. Only changes $\geq 1\,\%$ are shown.

Subregional patterns reinforce this contrast. In the Wet Chaco, flooded grasses and herbaceous vegetation contribute more than 36 % of BA, but tree cover still represents nearly one quarter, showing that fire activity extends beyond floodplain systems. In the Dry Chaco, shrublands dominate the burned LC composition ($\sim 39\,\%$), consistent with forest-to-shrub transitions shown in Fig. 5. In the Very Dry Chaco, fires overwhelmingly affect shrublands ($> 75\,\%$ of BA), reflecting both the current dominance of this cover type and its role in sustaining large fire events.

Fire-size distributions are strongly right-skewed in all subregions: more than 80 % of events fall within the Very Small ($< 1\,km^2$) and Small ($1–5\,km^2$) classes (Table S1; Fig. S6). However, larger fires contribute disproportionately to total BA. Megafires ($100–1000\,km^2$) are most frequent in the Wet Chaco, where continuous grassland and floodplain fuel beds favor fire spread during dry periods, whereas Gigafires ($> 1000\,km^2$) occur predominantly across shrublands in the Dry Chaco, where fuel structure and landscape openness facilitate extensive fire propagation.

Forest loss is widespread across the Chaco, particularly along deforestation frontiers in Argentina and Paraguay. However, the spatial association between recent forest loss and fire size differs regionally. In Argentina, deforestation fronts frequently coincide with clusters of small and medium fires, whereas in Paraguay and Bolivia fire activity is less concentrated along recent forest-loss edges. Across all regions, most large fires occur in non-forest areas. As shown in Fig. 5, many of these non-forest areas correspond to former tree-cover classes converted to shrublands and mosaic vegetation, linking forest degradation to the fuel structures that sustain larger fire events.

According to Fig. 6, the Wet Chaco registers the highest total burned area, nearly double that of the Dry and Very Dry regions. In this subregion, large fires contribute $\sim 40\,\%$ of annual BA, and small fires $\sim 20\,\%$ (Fig. S5). Despite their small individual extent, their high frequency ($> 36\,000$ fire events) results in a substantial cumulative contribution. Extreme years such as 2003 and 2020 were marked by widespread outbreaks.

In the Dry Chaco, fire count is lower, but large fires play a more prominent role. Large fires account for about 25 % of the annual BA, and gigafires can dominate totals in some years. For example, in 2019, just three gigafires in the Dry Chaco burned approximately $10\,000\,km^2$, equivalent to the region's mean annual BA and accounting for more than half of the total that year.

The Very Dry Chaco, while recording the lowest overall BA, exhibits abrupt interannual peaks driven by isolated megafires and gigafires, pointing to a more stochastic fire regime.

Between 2020 and 2022, the Wet Chaco experienced an unprecedented number of megafires and gigafires, both in terms of event counts and their contribution to total BA. These patterns align with the extreme fire weather anomalies described in Sect. 3.3.

3.3 Fire–weather relationship

Figure 7 presents the monthly BA climatology (2001–2022) with 2020–2022 overlaid for the Wet, Dry, and Very Dry

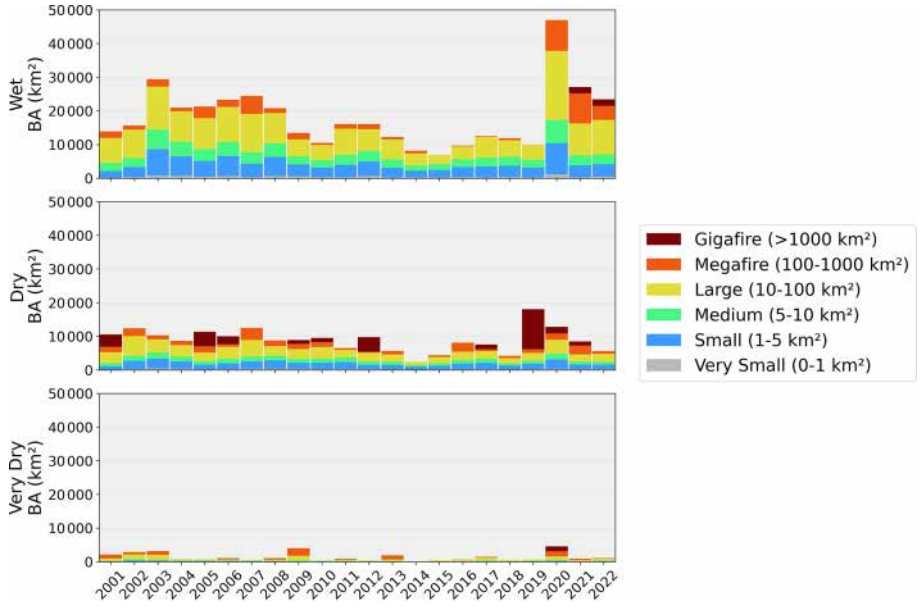

Figure 6. Cumulative burned area (2001–2022) by fire-size class across the Wet, Dry, and Very Dry Chaco subregions.

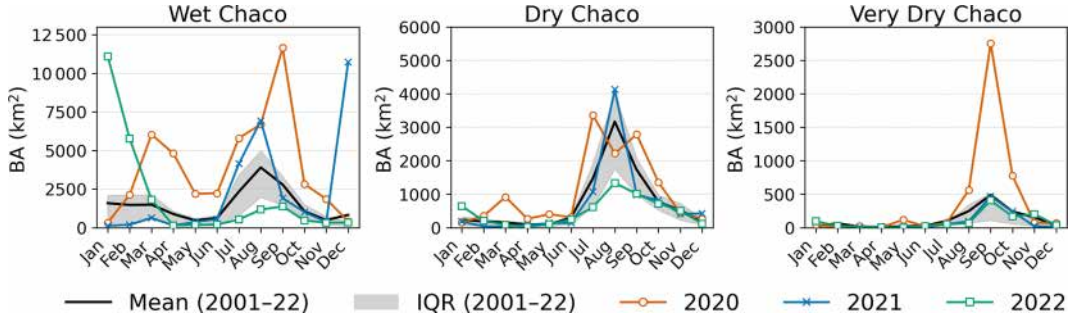

Figure 7. Seasonality of burned area (BA, km^2) in the Wet, Dry, and Very Dry Chaco. The black curve is the 2001–2022 monthly BA mean and the grey band shows the interquartile range (25 %–75 %). Colored curves overlay monthly BA for 2020 (orange circles), 2021 (blue crosses), and 2022 (green squares), highlighting differences from the climatological envelope. *Y*-axis limits differ by panel.

Chaco. In the Wet Chaco, BA in 2020 is above average for most months, with a secondary pulse in March–April (late wet season) preceding pronounced peaks in August–September (winter/dry season). In contrast, anomalies in 2021–2022 are concentrated in the summer/wet season (December–March), reaching levels similar to the typical late-winter/early-spring maximum, while post-winter months in 2022 remain mostly below average. In the Dry Chaco, 2020 stands out as extreme, particularly in July and September, whereas 2021 records an exceptional August at or above historical maxima and 2022 stays near or below the mean. In the Very Dry Chaco, positive anomalies are dominated by 2020, with a sharp September maximum; 2021 shows only minor increases, and 2022 remains subdued. Overall, 2020 shows widespread positive anomalies lasting several months across all subregions. In contrast, 2021 and 2022 generally feature shorter peaks, often concentrated in summer, although 2021 also records exceptional winter fires in the Dry Chaco. Activity during the canonical late-winter fire season is otherwise limited, particularly in 2022.

The spatial patterns of fire–weather coupling shown in Fig. 8 depict the per-pixel Pearson correlation between monthly Fire Weather Index (FWI) anomalies from ERA5-Land and BA anomalies derived from the gridded FRY dataset, both at 0.1° resolution, during the wet and dry seasons. FWI anomalies exhibit an approximately normal distribution, and after filtering pixels with fewer than four fire-active months, most BA anomaly series are quasi-normal, justifying the use of Pearson correlation as described in Sect. 2.3.7. Significant positive correlations ($p < 0.05$) are concentrated in the Wet Chaco, where R coefficients reach up to 0.7 during the wet season. In contrast, the Dry and Very Dry Chaco show weaker and more spatially scattered relationships, partly due to lower fire activity. Spearman cor-

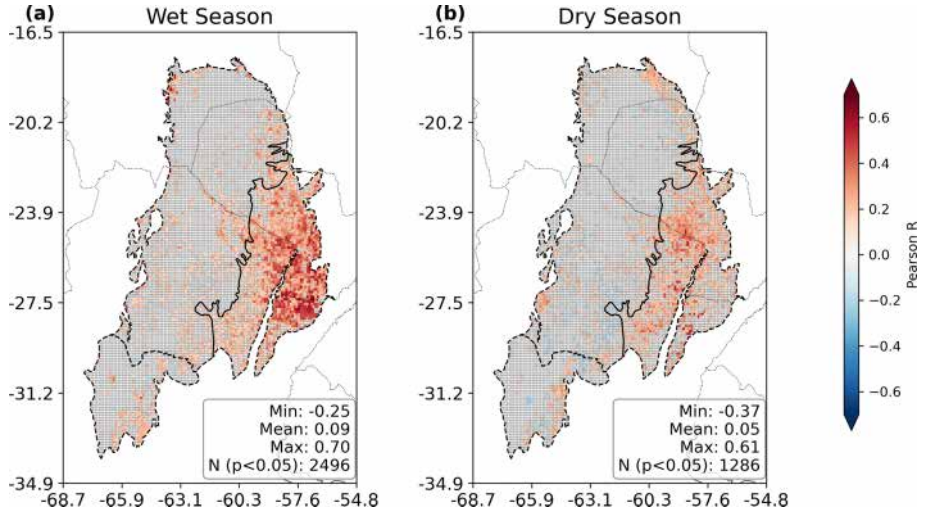

Figure 8. Spatial distribution of pixel-wise Pearson correlation coefficients between monthly Fire Weather Index (FWI) anomalies and monthly burned area (BA) for the period 2001–2022: **(a)** Wet Season and **(b)** Dry Season. The color bar indicates the strength and direction of the correlation (from negative in blue to positive in red). Inset statistics summarize the distribution of coefficients (Min, Mean, Max). Pixels marked with small black circles represent non-significant correlations (p-value > 0.05), while unmarked pixels indicate significant correlations (p-value < 0.05). Only pixels with more than 3-time steps with burned area > 0 were kept to avoid biased correlations related to very few or no fires.

relations were also calculated, resulting in similar patterns with lower coefficients (maximum R of 0.52; Fig. S7).

To further explore the spatial sensitivity of fire activity to fire weather, Fig. 9 compares per-pixel correlations between monthly FWI anomalies (see Sect. 2.3.7) and two metrics: fire counts and BA. Each dot represents a 0.1° grid cell, and quadrants classify response types. In the Wet Chaco, 93 % of cells fall in Q1, where both metrics show positive correlations with FWI, with moderate mean values (0.17 ± 0.12 for ignitions, 0.19 ± 0.13 for BA) and strong inter-metric correlation ($r = 0.76$). The Dry and Very Dry Chaco show more heterogeneous patterns, with Q1 proportions of 59 % and 61 %, and weaker mean correlations (~ 0.04–0.06). Still, inter-metric spatial correlations remain high ($r = 0.81$ and $r = 0.72$), indicating that regions more sensitive to fire weather in terms of ignitions also tend to be more sensitive in terms of fire extent.

Finally, the temporal co-evolution of annual BA and FWI anomalies is illustrated in the Supplement (Figs. S9–S10). Several years, especially in the Wet Chaco, show strong spatial correspondence between extensive fire activity and positive FWI anomalies (e.g. 2012, 2020–2022). However, other years (e.g. 2003) reveal extensive BA without matching FWI extremes, underscoring that weather is not the sole driver of interannual variability.

3.4 Temporal dynamics of fire–environment interactions

To explore how conditions evolve before and after fire events, we analyzed both regional time series and lagged correlations between BA anomalies and three key drivers: FWI, rainfall, and vegetation greenness (EVI), over the period 2001–2022 (Figs. 10 and S10).

The time series analysis (Fig. S10) reveals a coherent pattern in all subregions. Typically, positive rainfall anomalies (which automatically decrease FWI) are followed by increased EVI, indicating vegetation growth and fuel accumulation. When this is then followed by elevated FWI values (due to negative rain and humidity anomalies, extreme heat and/or strong winds), peaks in BA are frequently observed. This pattern supports the interpretation of a fire-favoring sequence: moisture enables biomass build-up, which is later dried and made flammable under high fire-weather conditions, culminating in fire activity. This cycle is particularly evident in major fire years such as 2020 and 2022, especially in the Wet Chaco, where the alignment between environmental anomalies and BA peaks is striking. In the Dry and Very Dry Chaco, the sequence is also well defined, although slightly more variable probably due to limited fuel accumulation.

The influence of large-scale climate variability, particularly the El Niño–Southern Oscillation (ENSO), is also reflected in the fire–environment dynamics. During La Niña phases (negative ENSO), we observe reduced rainfall and elevated FWI values, often coinciding with increased BA. Conversely, El Niño episodes (positive ENSO) are associated with wetter conditions, lower fire-weather pressure, and reduced fire activity (Figs. S10 and S11).

Figure 10 shows lagged Pearson correlations between monthly anomalies of BA and FWI, rainfall, and EVI for the

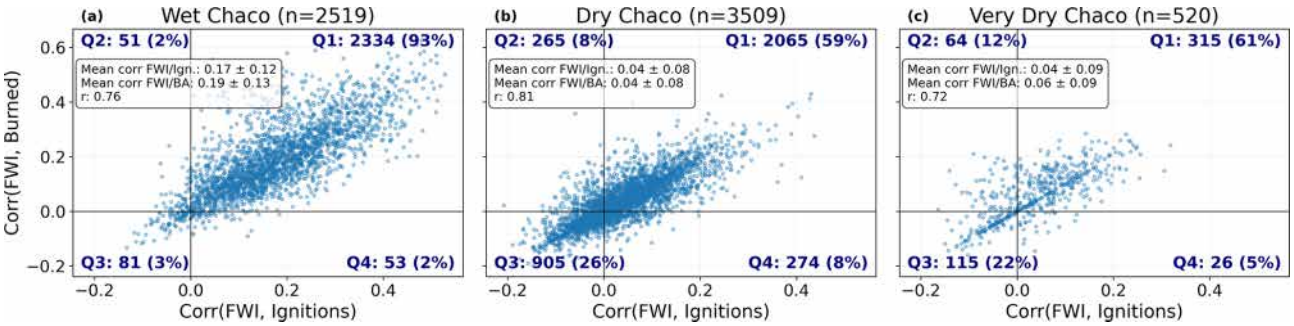

Figure 9. Each panel shows a scatterplot of per-pixel Pearson correlation coefficients between the Fire Weather Index (FWI) and two fire activity metrics – ignition frequency (x-axis) and burned area (y-axis) – over the period 2001–2022. The panels correspond to the Wet, Dry, and Very Dry Chaco subregions, and each dot represents a $0.1° \times 0.1°$ grid cell. Quadrants are defined by the sign of each correlation coefficient to classify spatial patterns of fire–weather association: Q1 (top-right) includes pixels with positive correlations for both ignitions and burned area; Q3 (bottom-left) includes negative correlations for both; Q2 and Q4 represent divergent cases. For each subregion, quadrant counts, percentages, and summary statistics (mean ± standard deviation of each correlation axis and Pearson r between them) are annotated.

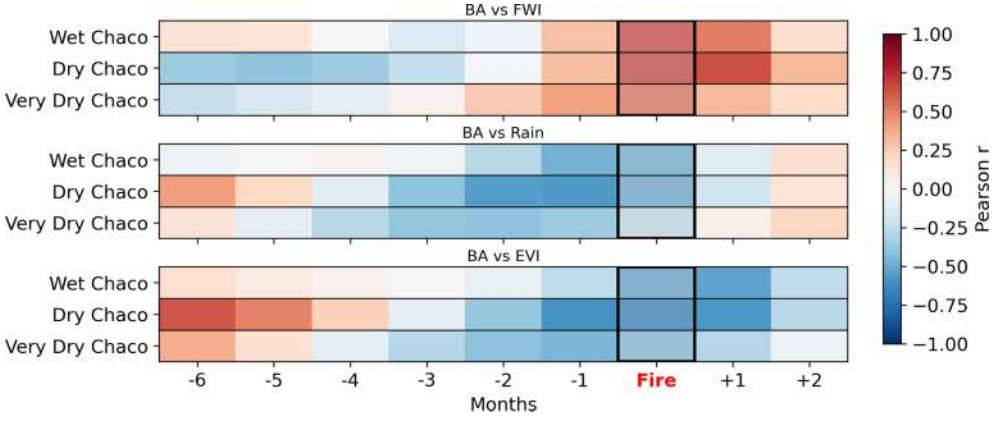

Figure 10. Lagged correlations between monthly anomalies of FWI, rainfall, and EVI with burned area in the Gran Chaco. Each heatmap shows the Pearson correlation coefficient between the anomaly of a given variable (FWI, rainfall, or EVI) at different time lags and the burned area anomaly, for each Gran Chaco subregion. Negative lags indicate the variable leads burned area; positive lags indicate it follows. Correlations are computed from pixel-based, region-averaged monthly time series for 2001–2022.

three Chaco subregions. Positive correlations between BA and FWI at lags 0 to +1 months, indicate that peak fire activity coincides with high fire-weather conditions. Rainfall and EVI display negative correlations with BA at short negative lags (−1 to −3 months), consistent with dry, senescent vegetation promoting flammability. At longer negative lags (−5 to −6 months), especially in the Dry and Very Dry Chaco, both variables correlate positively with BA, suggesting that wetter, greener periods months earlier promote fuel build-up. In the Wet Chaco, lag correlations are weaker and less structured, likely due to consistently moist conditions that buffer fire–environment coupling.

3.5 Fire-weather types

To characterize the atmospheric conditions associated with fire occurrence and fire growth, we analyzed the Fire–Weather Types (FWTs) assigned to each fire patch during the days preceding ignition (Pre-Fire clusters) and during the active burning period (During-Fire clusters). Figure 11 presents the spatial distribution and frequency of the three FWT categories (Neutral, Drought Driven and Wind Driven) for both clustering types.

Neutral FWTs dominate both clustering groups, but their share decreases from 50.9 % to 45.3 % overall, while Drought-Driven rises from 26.6 % to 30.8 % and Wind-Driven from 22.4 % to 23.9 % (Figs. 11c–d and S12). This indicates that when fires are clustered according to the meteorology during the fire rather than before ignition, a larger fraction falls into drought or wind related conditions and fewer remain neutral. In the Wet Chaco, Neutral FWTs drop from 49 % to 42 % with a marked increase in Drought-Driven; in the Dry Chaco, both non-neutral types grow moderately; in the Very Dry Chaco, Wind-Driven types increase sharply (from 15 % to 26 %), especially in the south where complex topography may strongly influence fire–atmosphere

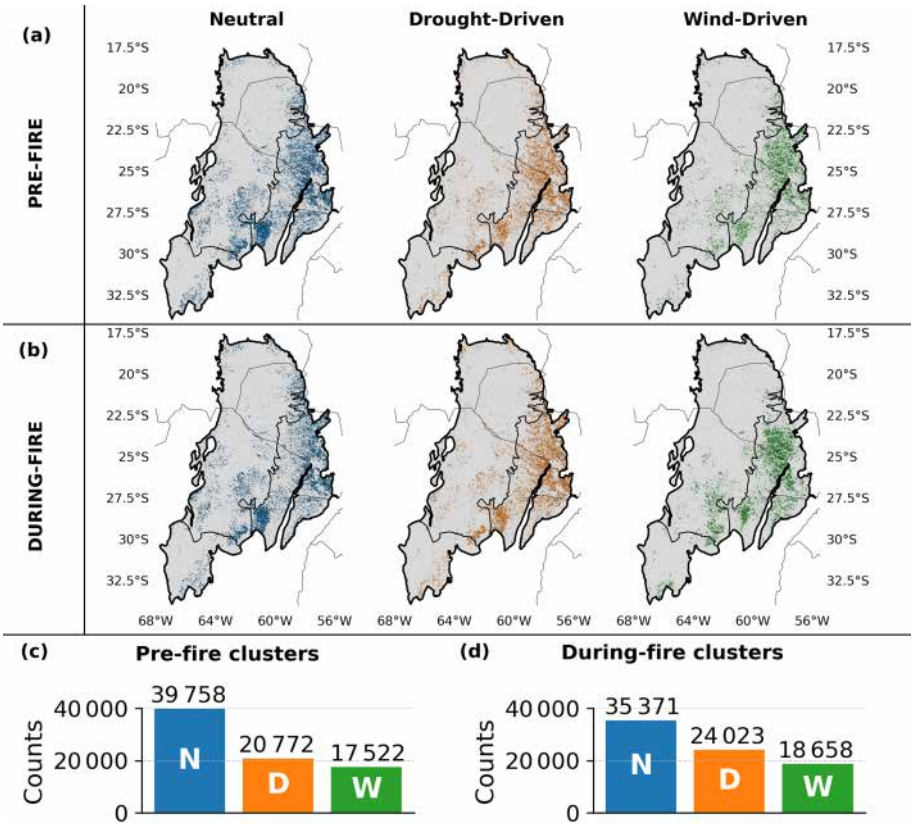

Figure 11. Spatial distribution and frequency of pre- and during-fire meteorological clusters across the Gran Chaco (2001–2022). Panels **(a)** and **(b)** show the geographic location of fire patches classified into three Fire–Weather Types (FWTs) – Neutral (blue), Drought-Driven (orange), and Wind-Driven (green) – for the pre-fire and during-fire periods, respectively, overlaid on Chaco sub-region boundaries Some patches overlap through the years and may partially or totally cover each other. Panels **(c)** and **(d)** display the total number of patches assigned to each FWT for pre-fire and during-fire clustering methods, respectively.

dynamics (see Sect. 2.1). These regional shifts suggest that dryness is particularly important in the Wet Chaco, while stronger winds become comparatively more relevant in the southern Very Dry Chaco.

Figure 12 shows mean daily anomalies from 20 d before to 20 d after ignition for each FWT for both clustering types. In the Pre-Fire FWT, we see that the Wind-Driven fires present a sharp rise in wind speed and temperature in the days around ignition, coupled with a drop in RH, creating highly flammable conditions. Drought-Driven fires exhibit a long build-up of dryness before ignition, with persistently high DC and DMC values and low RH, indicating extended fuel curing. Neutral fires occur under conditions close to climatology, with only small fluctuations in all variables.

The time series of the During-Fire FWTs show that the dry conditions characteristic of the Drought-Driven cluster begin to develop before ignition and remain well differentiated during the fire, with very low RH and high DC and DMC values. Wind speed anomalies are also elevated in this cluster, although not as sharply as in the Wind-Driven cluster. This indicates that dryness and wind can co-occur in Drought-Driven fires, whereas Wind-Driven fires are characterized by a clear and sustained peak in wind speed combined with dry conditions, but without the prolonged build-up of drought observed in the Drought-Driven cluster. The Neutral cluster remains close to climatology throughout, with only a slight decrease in RH immediately prior to ignition, suggesting a minimum dryness threshold for fire initiation across clusters.

When comparing FP morphology across clusters, Pre-Fire FWTs appear broadly similar (Figs. 13, S13–S14), with comparable FP area, shape index (deviation from compactness), core-area index (interior cohesion), eccentricity (elongation), and perimeter-to-area ratio (boundary complexity). In contrast, During-Fire FWTs show clear differences: Wind-Driven fires tend to be larger, more elongated (higher eccentricity), and more cohesive (higher core-area index and lower perimeter-to-area ratio) than Drought-Driven fires, consistent with a directional spread under strong and sustained winds.

The combination of high eccentricity and low perimeter-to-area ratio reflects elongated but relatively smooth fire perimeters produced by the rapid advancement of the fire under strong winds. In contrast, Drought-Driven fires tend to

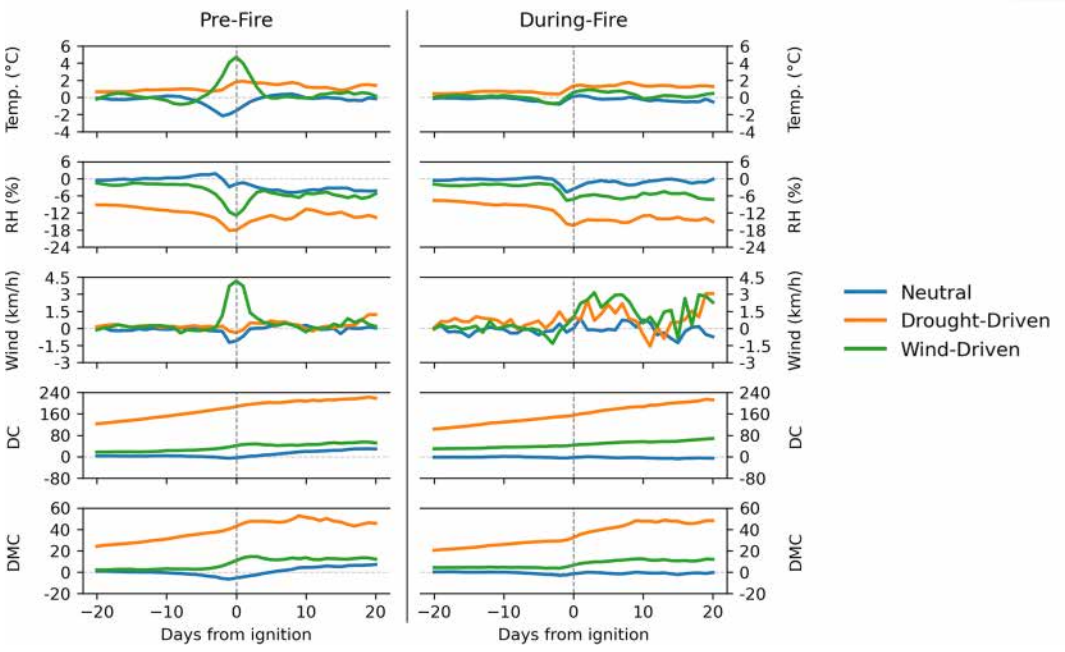

Figure 12. Mean daily anomalies of temperature (Temp.), relative humidity (RH), 10 m wind speed, Drought Code (DC), and Duff Moisture Code (DMC) from 20 d before to 20 d after fire ignition, averaged over fire patches assigned to the Neutral, Drought-Driven, and Wind-Driven clusters for Pre-Fire (left) and During-Fire (right) clustering approaches.

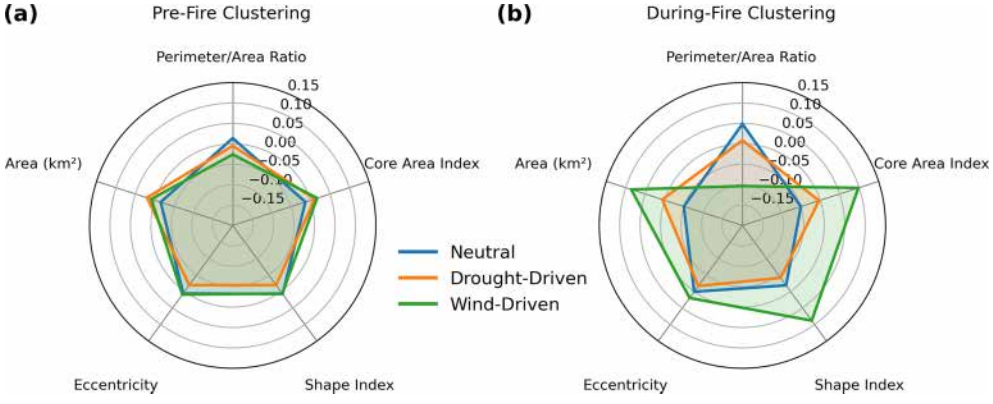

Figure 13. Clusters mean morphology profiles for **(a)** Pre-Fire and **(b)** During-Fire clustering. Each axis represents a standardized morphology variable (z-score), and each colored polygon shows the mean profile for one cluster. The radial extent indicates the relative value of each variable within the dataset.

generate more irregular boundaries for a given size, consistent with a stronger dependence on the spatial distribution of cured fuels, which causes the fire to advance unevenly across fuel patches and results in more complex and less smooth perimeter shapes.

Overall, Pre-Fire FWTs capture the atmospheric conditions leading to ignition, whereas During-Fire FWTs better reflect the conditions that shape the eventual size and geometry of the fire. These results show that both clustering types capture different aspects of fire–weather interactions, but that the During-Fire FWTs provides clearer separation in terms of final fire size and morphology.

3.6 Fire size drivers

Our RF analysis identified static topographic and vegetation structure variables as the dominant predictors of final fire size in the Gran Chaco (Fig. 14a). Mean elevation showed the highest mean SHAP value (17.4 %), followed by LC evenness (10.8 %), tree/shrub/herbs mosaics (9.79 %) and mean slope (9.1 %). These four variables consistently occupied the top positions across the global model and all twelve specific models (Fig. 15). LC fractions within the FPs, including cropland or flooded herbaceous cover, made moderate contributions, whereas meteorological and social variables

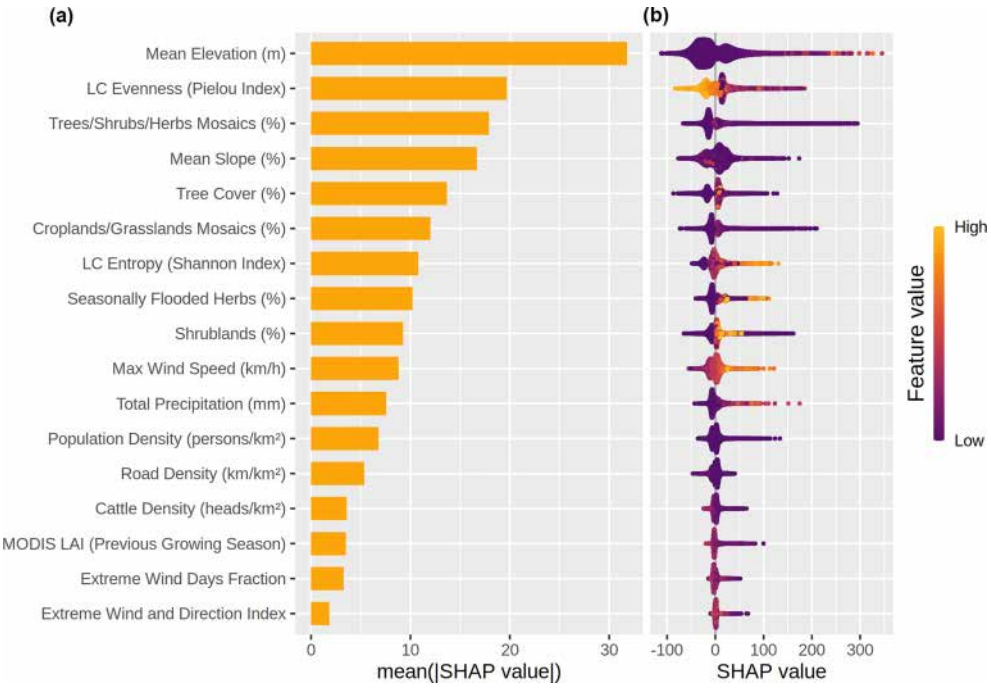

Figure 14. Feature importance ranking for the Random Forest model predicting fire patch (FP) size across the entire Gran Chaco. **(a)** shows the average importance of each variable, expressed as the mean absolute SHAP value, which reflects how strongly each feature contributes to model predictions on average. **(b)** shows the SHAP values for all individual fire patches, indicating how low (purple) or high (yellow) feature values influence the prediction toward smaller or larger fires. SHAP values are used here to quantify feature importance consistently across the dataset.

such as maximum wind speed, precipitation, population density or cattle density ranked markedly lower in importance. Figure 15 demonstrates that this hierarchy is almost unchanged across regional, seasonal and fire-weather subsets, stable across all model configurations.

Model performance was satisfactory, with the global RF achieving a correlation of 0.74 on the test set and a test RMSE of ~ 110 burned pixels, compared with 0.96 and ~ 54 pixels on the training set (S14). These values indicate limited overfitting and show that the model captures a substantial fraction of the variance in fire size despite the inherent noise and strong skewness of the response variable. Because the target variable is the number of burned FRY pixels within each FP, RMSE values are interpreted directly in pixel units; with the 250 m FireCCI51 resolution, 110 pixels correspond to approximately 6.9 km^2, less than 7 % of the 1–100 km^2 size range analyzed here. Comparable performance was obtained across all regional, seasonal and fire-weather configurations (Table S3).

Predictor distributions were often skewed (Table S2; Fig. S15), which is reflected in the SHAP spreads and dependence patterns. The global SHAP distribution (Fig. 14b) shows that elevation exerts a consistently positive influence on predicted fire size across most of its range, with the PDP in Fig. 16 revealing a steep rise in SHAP values between 0 and $\sim$40–60 m, followed by a broad plateau. Large fires dominate this low to mid elevation interval, while higher elevations generally host smaller events. This pattern reflects major physiographic contrasts in the Chaco, including low-lying floodplains and seasonal wetlands ("esteros" and "bañados") versus slightly elevated terraces ("montes", "albardones") covered with woody vegetation (Bravo et al., 2025).

Regional PDPs (Figs. S17–S19) show the same elevation signal with different thresholds. In the Wet Chaco, SHAP values rise sharply from 0 to $\sim$20–40 m and stabilize above that threshold, while in the Dry Chaco the increase is concentrated in the 0–20 m band and flattens near 50–100 m. In contrast, the Very Dry Chaco exhibits a nearly linear positive gradient up to $\sim$700 m, with large fires clearly associated with higher elevation.

Mean slope refines this topographic signal. Although its global importance is slightly lower than elevation, its SHAP dependence curve (Fig. 16) mirrors the elevation-driven distinction between flat floodplain fuels and more fragmented uplands. SHAP values decline sharply between 0 and $\sim$2 %–3 % slopes, where the largest fires are concentrated, and then stabilize. In the Wet and Dry Chaco, large fires are almost entirely confined to slopes below $\sim$2 %–3 % (Figs. S17–S19), whereas steeper terrain hosts only small fires. The Very Dry Chaco departs from this pattern, showing a monotonic nega-

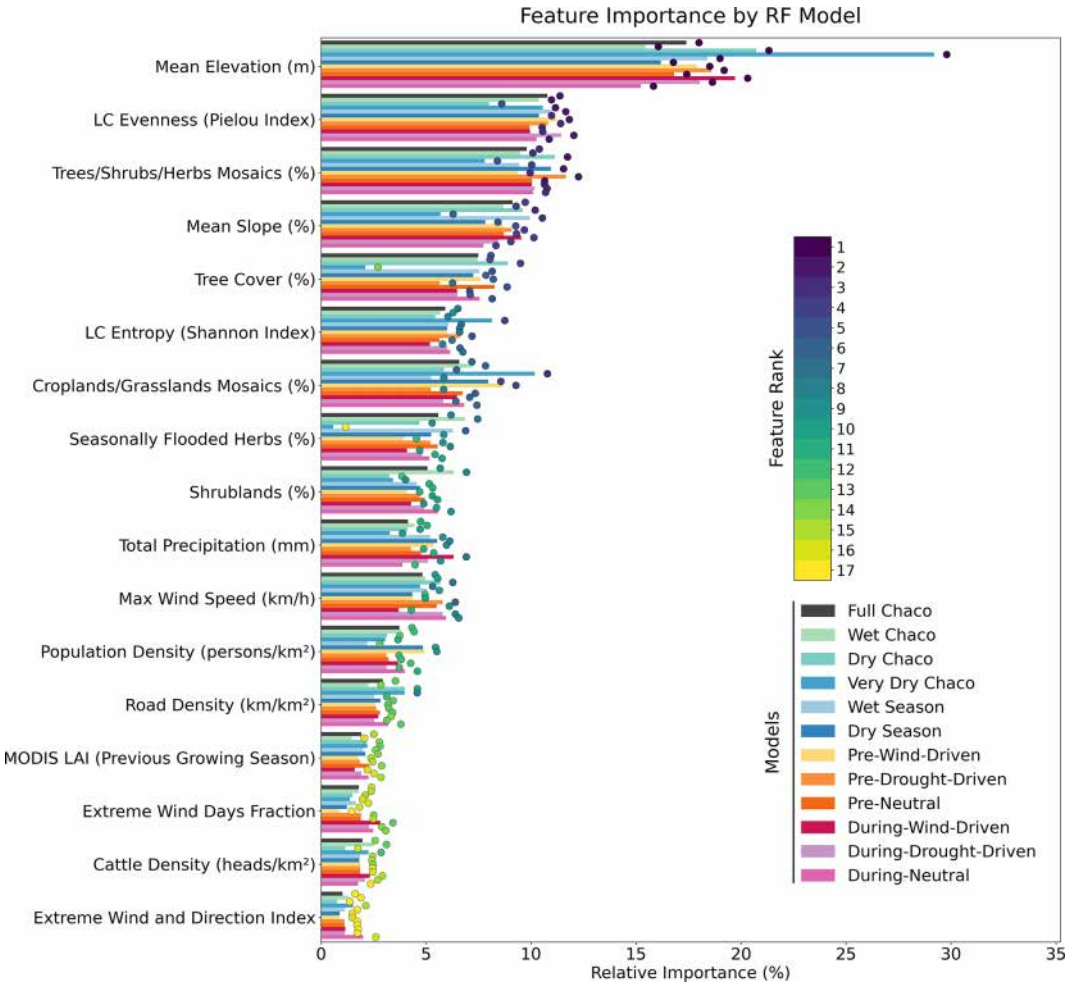

Figure 15. SHAP feature importance ranks across all trained Random Forest models used to predict fire patch size (n_cell) based on 17 explanatory variables. Colored dots at the end of bars shows the rank of a variable's importance (1 = most important, 17 = least important) for a given model.

tive gradient with a small cluster of large fires at intermediate slopes (∼ 20 %–30 %).

LC evenness and LC entropy display opposite but complementary patterns as two metrics of landscape heterogeneity. Evenness decreases when one or two land-cover classes dominate the patch, whereas entropy increases with the number and diversity of cover types, even when their proportions are uneven. Both indices are zero when only one class is present. In the global SHAP summary (Figs. 14b and 16), many of the largest fires occur where a dominant class (low evenness) coexists with several secondary LC types (intermediate entropy).

Across subregions, the same evenness–entropy structure emerges (Figs. S17–S19). Evenness shows a consistently negative SHAP gradient across the Wet, Dry and Very Dry Chaco, with the transition to negative contributions near 0.6 in all regions, although small and large fires occur across the full range, indicating modulation rather than strict control. Entropy exhibits a more complex U-shaped structure regionally, with SHAP values decreasing up to ∼ 0.2 and rising toward intermediate entropies, where large fires concentrate, before declining again at high entropy values, where only small fires are observed. Overall, larger fires occur most frequently at intermediate heterogeneity levels.

LC fractions modulate fire size and their SHAP dependence patterns (Figs. 14b, 16, S17–S19) are consistent with the heterogeneity indices described above. The tree–shrub–herb mosaic class shows a strong and monotonic negative relationship with fire size across the entire Gran Chaco and in all three regions: high fractional cover of mosaics systematically shifts SHAP values toward smaller fires, whereas the largest fires appear at lower fractions of the mosaic class. Because mosaics are represented as a single categorical class in CCI-MRLC, patches dominated by mosaics behave as homogeneous units in the evenness and entropy indices because they count as a single LC class. Tree cover displays a broadly

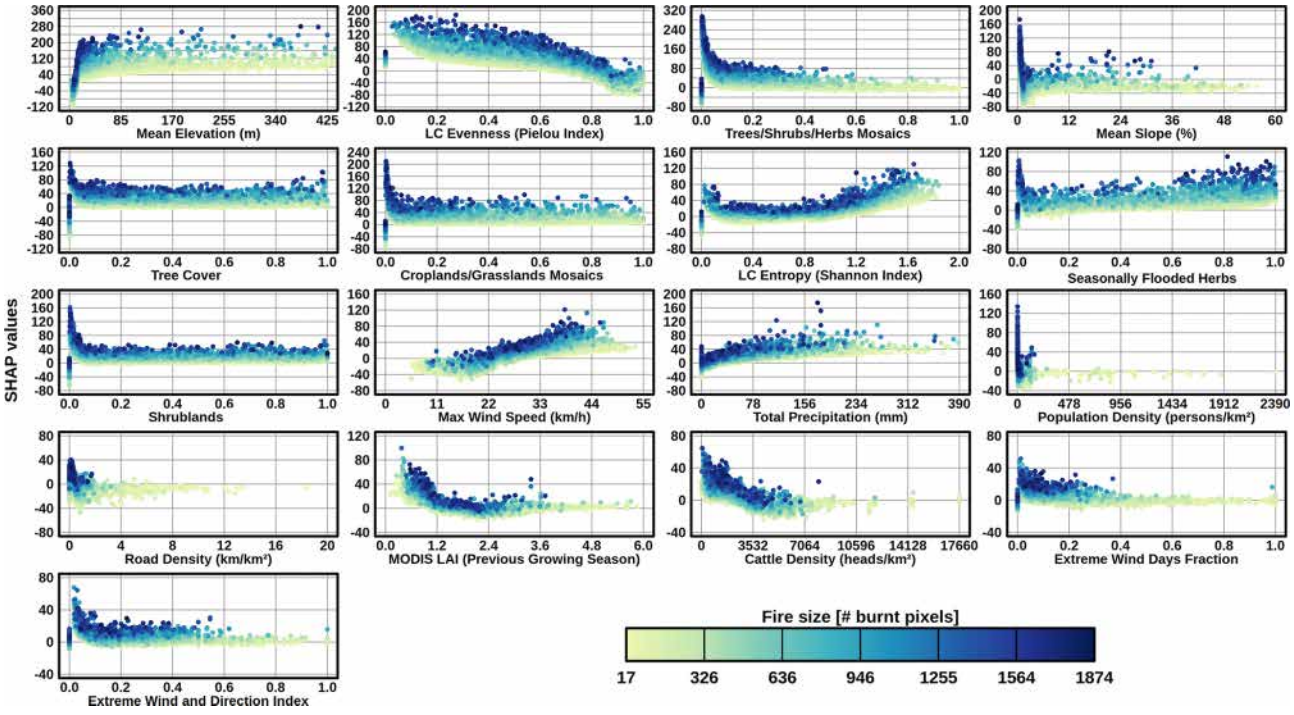

Figure 16. SHAP dependence plots for the 17 explanatory variables used to predict fire patch size (*n*_cell) with the Random Forest model trained on fire patches between 1 and 100 km^2 in the entire Gran Chaco between 2001 and 2022. Each panel shows the SHAP value (*y*-axis) across the range between 0 and the 0.995 quantile of a given feature (*x*-axis), illustrating the marginal effect of that feature on the model's output. Dots are colored by fire size (number of burned pixels), with darker tones indicating larger fires. Land cover classes represented as fractions.

similar negative trend in the global model and in the Wet Chaco. The regional PDPs add two nuances: in the Very Dry Chaco the decline in SHAP values is nearly linear across the tree-cover gradient, whereas in the Dry Chaco a secondary rise in SHAP values at high fractional tree cover suggests the presence of large fires in recently deforested or thinly wooded areas still mapped as forest.

Shrublands exhibit contrasting SHAP responses across subregions. In the global model and in the Wet Chaco, shrub fractions show a steep negative exponential decay, with the largest fires concentrated at low shrub cover and exclusively small fires at high shrub dominance. The Dry Chaco shows the opposite pattern: SHAP values increase with shrub cover. The Very Dry Chaco exhibits a distinct, strongly non-linear shape, with SHAP values stable at low and intermediate shrub fractions but increasing sharply around $\sim$0.8–0.9, before declining at the extreme upper tail.

Flooded herbaceous vegetation shows a mixed response globally: SHAP values initially decrease between 0 and $\sim$0.1 but become increasingly positive toward higher fractions, indicating that fires occurring in seasonally desiccated wetlands often reach large sizes. This flooded-herbaceous effect is concentrated in the Wet Chaco (dark points at high fractions) and is negligible in the Very Dry Chaco (large fires only where flooded cover is $\sim$0; Figs. S17–S19). Cropland/grassland mosaics mirror the global shrubland pattern, with a clear negative exponential relationship in all regions: large fires almost exclusively occur at low fractions, whereas patches dominated by these mosaics generate small fires.

The influence of pre-fire biomass accumulation, represented by previous-season LAI, is modest in global importance but shows consistent region-specific patterns that reflect its role as a broad proxy for vegetation productivity (Figs. 16; S17–S19). At the scale of the entire Gran Chaco, SHAP values decrease strongly from low to moderate LAI, with the largest fires concentrated at LAI $<$ 1–1.5. Higher LAI values correspond to increasingly negative SHAP contributions across all regions. The regional PDPs clarify how this proxy behaves along the gradient (Figs. S17–S19): in the Wet Chaco, increases in LAI coincide with vegetation types that tend to reduce spread regardless of their biomass; in the Very Dry Chaco, the compressed LAI range reflects lower overall productivity (0–4 vs 0–6 in the other regions), and large fires remain associated with the lowest values; in the Dry Chaco, a weak secondary rise in SHAP values at intermediate LAI, forming a U-shape curve.

Meteorological predictors show consistent but secondary influences relative to topography and vegetation structure (Figs. 14b, 16, S17–S19). Maximum wind speed exhibits the clearest signal: SHAP values increase steadily with maxi-

mum wind speed up to roughly 40–45 km h^{-1}, beyond which they form a plateau. In all regions, large fires cluster toward the upper half of the wind-speed distribution. In the FWT-specific RF models, this effect becomes more prominent in Drought-Driven configurations, where maximum wind speed attains higher SHAP-based importance ranks and larger absolute SHAP amplitudes than in Neutral or Wind-Driven FWTs (Fig. 15).

In contrast, the two extreme-wind metrics (extreme wind days fraction and extreme wind-and-direction index) display weak negative or near-flat SHAP responses. SHAP values decline from slightly positive to near-zero between fractions of 0 and ~ 0.2, after which only small fires occur in all regions. The Very Dry Chaco shows a shallow positive segment at very low fractions but converges toward the same pattern.

Total precipitation shows uniformly weak contributions across regions. Although the global SHAP curve appears moderately positive at low to intermediate precipitation totals, large fires are clearly concentrated at low rainfall values across subregions (Figs. S17–S19), and small fires dominate wetter intervals. The apparent positive SHAP slope at low to intermediate precipitation values reflects the construction of the predictor, which integrates rainfall over the fire duration. Because longer-lasting fires accumulate more rainfall within the event window, this variable is partially confounded with fire duration. This structural coupling explains why some large fires appear at intermediate precipitation totals despite the overall concentration of large events at low rainfall. Thus, precipitation contributes only marginally to the RF predictions once static fuel and topographic structure are accounted for.

Human-pressure variables (road density, population density, cattle density) have consistently low mean SHAP importance across all RF models (Fig. 14a), indicating that they explain only a minor portion of the variance in fire size once topography and vegetation structure are accounted for. Nevertheless, their marginal SHAP responses (Figs. 16, S17–S19) reveal systematic gradients that are interpretable in a fire-management context.

Cattle density shows the clearest pattern: SHAP values decline almost monotonically with increasing cattle density, and the largest fires are concentrated at low to moderate densities. At high densities, SHAP values are strongly negative and large fires are absent. High stocking rates reduce standing biomass and fuel continuity, limiting the capacity of fires to spread into large patches. This trend is constant across all regions.

Road density and population density exhibit parallel patterns. SHAP values are positive at low densities and become increasingly negative as infrastructure or settlement density increases. Large fires occur almost exclusively where road and population density are low, whereas high-density areas are dominated by small fires.

Despite these coherent marginal trends, the overall contribution of human-pressure variables remains secondary. Their effects are largely overshadowed by static topographic structure and LC composition, and their marginal signals do not alter the dominance hierarchy observed in Fig. 15. Overall, human-pressure proxies contribute modestly once topography and vegetation structure are accounted for, and they do not alter the dominant predictor hierarchy.

3.7 Sensitivity experiments

To assess the robustness of the models and the sources of explanatory power, we performed two targeted sensitivity experiments: (i) training a RF without topographic variables, and (ii) replacing the baseline road density product with an alternative dataset containing more detected road features.

In the No-Topography experiment, the overall ordering of non-topographic predictors remained stable (Fig. S20): vegetation-structure metrics (LC evenness, mosaic cover, tree cover, LC entropy) continued to dominate, while human-pressure and weather variables remained secondary. Despite this stability in feature hierarchy, removing topography resulted in a marked decline in predictive performance (test COR decreasing from ~ 0.74 to ~ 0.67; test RMSE increasing from ~ 110 to ~ 119 pixels; Table S3). SHAP rankings also became less coherent, with several land-cover variables inflating artefactually in importance to compensate for the absence of structural information. These changes confirm that elevation and slope do not act as direct physical drivers but capture slow-varying ecological gradients that distinguish floodplain herbaceous systems from slightly elevated woody landscapes, which strongly condition the potential for large fire growth.

Although the MS road dataset detects substantially more minor linear features than OSM (see Supplementary Section S2 for detailed comparison), substituting OSM with MS in the RF models produced negligible changes in predictive performance and no change in feature rankings. Test COR remained at 0.74 and test RMSE shifted only marginally (Table S3). Road density retained similarly low mean SHAP importance (2 %–3 %), and SHAP dependence curves were nearly identical across both datasets. This indicates that the additional fine-scale detail captured by MS does not provide independent explanatory power for final fire size at the regional scale.

Taken together, these results confirm three key points: (i) road density is strongly collinear with land-cover composition and landscape heterogeneity; (ii) aggregating road metrics at the patch level reduces sensitivity to fine-scale differences between datasets; and (iii) once other landscape variables are accounted for, road density contributes only marginally to explaining final fire size at the regional scale. Accordingly, substituting the road dataset does not materially affect predictive performance or feature ranking. Thus, neither road dataset (OSM nor MS) provides independent explanatory power beyond that already captured by topography and LC.

4 Discussion

Building on event-level fire patches (FPs), we examine how meteorology, landscape structure, and human pressures shape fire size and morphology across the Wet, Dry, and Very Dry Chaco.

4.1 Fire regime and extreme events

FP data reveal a strongly skewed size distribution: many small fires ($< 5\,km^2$) and a few very large events that dominate burned area (BA), consistent with global patterns (Archibald et al., 2009; Hantson et al., 2015, 2017; García et al., 2022; Haas et al., 2022). Megafires ($> 100\,km^2$) are most frequent in the Wet Chaco, where continuous herbaceous fuels in savannas and seasonally flooded vegetation support spread. Gigafires ($> 1000\,km^2$), although rare, occur predominantly in the Dry Chaco and are often concentrated in remote areas where suppression access may be limited, and where seasonally cured fuels and low humidity can favor sustained spread.

In the Gran Chaco, most ignitions are human-caused and fire use remains widespread across rural activities (Bravo et al., 2010, 2025), so the spatial and temporal distribution of fire occurrence largely reflects anthropogenic pressure. However, once a fire is ignited, its final size depends more strongly on fuel continuity, landscape structure and fire-weather conditions than on ignition source. Human pressures and their proxies are discussed in Sect. 4.5.

Feron et al. (2024) show that the Gran Chaco region in South America has experienced an increase in the frequency of warm, dry and flammable days, together with a rise in compound warm-dry anomalies over recent decades. Although these diagnostics do not quantify fire behavior, they indicate a background shift toward more frequent atmospheric conditions conducive to high flammability. In our record, 2019–2022 coincides with strongly positive FWI anomalies and multiple large fire years, particularly in the Wet Chaco. Despite the overall decline in BA between 2001 and the mid-2010s, the clustering of extreme years at the end of the time series is consistent with increasing exposure to periods of elevated fire weather under recurrent drought and large-scale climate variability (e.g. intensified La Niña conditions), while noting that the satellite era remains short for robust trend detection.

Extreme fire periods, such as the 2019–2022 season, illustrate this sensitivity. In our record, a handful of very large fires contributed a substantial share of total BA across the three subregions. This pattern aligns with reconstructions of twentieth-century fire activity showing that the Gran Chaco woodlands experience relatively frequent but generally low-to-moderate severity fires, with large fire seasons emerging when fuel accumulation coincides with prolonged dry periods (Bravo et al., 2021, 2025; San Martín et al., 2023; Vidal-Riveros et al., 2023). During 2019–2022, multi-year drought affected large parts of the La Plata basin, including the Gran Chaco, reducing river discharge, soil moisture and wetland extent (Naumann et al., 2023). Consistent with this hydroclimatic context, we observe widespread positive BA anomalies and high FWI, particularly during 2020–2021 and especially in the Wet Chaco, where rivers and floodplains typically constrain lateral spread.

Additionally, as discussed in the Introduction, the COVID-19 pandemic altered mobility, enforcement and on-the-ground fire management across South America, with contrasted effects on fire activity depending on whether restrictions reduced ignitions or weakened surveillance and suppression (Garcia et al., 2021; Eklund et al., 2022; Kumar et al., 2022; Naval Fernández et al., 2023). In the Gran Chaco, mobility declined during peak fire months, yet suppression capacity remained relatively stable due to the continued availability of volunteer brigades, while agrarian expansion and land-clearing dynamics, including deforestation burns and infrastructure projects, continued during lockdown (Castilla, 2021; Naval Fernández et al., 2023; Schmidt and Castilla, 2023). Together, these observations indicate that the persistence of extreme fire seasons during 2020–2022 cannot be explained solely by pandemic-related changes in human activity, and that concurrent drought and elevated fire weather likely played a central role in enabling large fire spread.

We therefore examined how short-term fire weather relates to BA across subregions and found strong spatial contrasts consistent with a fuel-limited to moisture-limited continuum across the Gran Chaco. In the Wet Chaco, high FWI is consistently associated with large BA, confirming moisture limitation and strong sensitivity to atmospheric conditions, in line with earlier BA-based analyses (San Martín et al., 2023) and with varying-constraint frameworks across resource gradients (Krawchuk and Moritz, 2011).

In the Dry and Very Dry Chaco, correlations are weaker and more heterogeneous, indicating partial decoupling between short-term fire weather and final size, with FWI effects mediated by antecedent fuel conditions and landscape continuity, consistent with evidence that wildfire activity peaks at intermediate rainfall and productivity levels in semiarid Chaco landscapes, where fuel loads are sufficient but seasonal curing remains pronounced (Bravo et al., 2010; Argañaraz et al., 2015; San Martín et al., 2023).

Lagged relationships reinforce this contrast: in drier areas, positive rainfall and vegetation productivity 4–6 months before fire are followed by higher BA once fuels cure, supporting the fire–productivity hypothesis (Pausas and Bradstock, 2007) and matching wet-to-dry sequences linked to widespread burns in western and central Chaco forests (Bravo et al., 2010; Argañaraz et al., 2015; San Martín et al., 2023), whereas in wetter areas short dry spells immediately prior to fire are more predictive of activity because fuels are rarely limiting (Krawchuk and Moritz, 2011).

4.2 Fire-weather types across the Chaco region

To assess how daily fire weather influences fire size, we built on the framework of Hernandez et al. (2015) and Ruffault et al. (2016, 2020), who classified Mediterranean wildfires into Fire-Weather Types (FWTs) based on pre-fire meteorological anomalies (heat, drought, wind) and found that Hot-Drought and Wind-Driven types were strongly linked to large events. Applying a similar pre-fire clustering in the Gran Chaco (Neutral, Drought-Driven, Wind-Driven) captured ignition contexts but explained little variation in final size or shape. This limited explanatory power is consistent with flat, fuel-rich systems where pre-fire anomalies modulate the probability of fire occurrence but do not reliably predict how far fires will spread once ignited.

In contrast, clustering based on during-fire variables (maximum wind speed, total precipitation, drought indices, and the Extreme Wind and Direction Index developed in this study) clearly separated groups with significant differences in size and morphology. Dry, windy days during the fire, favored rapid and large expansion.

Our findings contrast with Ruffault et al. (2016, 2020) and Belhadj-Kheder et al. (2020), who found pre-fire or near-ignition anomalies predictive in Mediterranean and North African settings, respectively, with the latter highlighting anomaly duration in low-suppression contexts. The stronger size–weather link for during-fire meteorology that we found likely reflects Chaco-specific traits such as a relatively flat terrain, continuous fuels, and permissive fire conditions (Bucher, 1982; Vidal-Riveros et al., 2023), which make wind and humidity more decisive than pre-fire anomalies. In the Mediterranean, fragmented fuels, complex topography, and strong suppression (Ruffault and Mouillot, 2015, 2017), translate into ignition-day extremes mattering more. A similar modulation by suppression capacity occurs in western U.S. forests (Higuera et al., 2015).

In semiarid mountain landscapes of the Very Dry Chaco, Argañaraz et al. (2015) showed that climatic gradients and productivity govern where fires tend to occur, while topography and land-use mosaics constrain their spatial extent. Although their study addressed fire frequency rather than fire size, the distinction reinforces that the drivers of fire occurrence and the drivers of fire spread are related but not identical, and that landscape context mediates how daily fire weather translates into final fire extent.

Our clustering extends fire-weather typologies to a tropical dry forest context and complements recent Gran Chaco regime classifications (Vidal-Riveros et al., 2024; Naval-Fernández et al., 2025) that omitted meteorological variables, highlighting the key role of fire-active weather in shaping fire morphology.

These fire-weather patterns operate within a landscape where ignitions are predominantly anthropogenic, meaning that, aside from the few lightning-ignited events, human activities largely determine when and where fires start. The eventual size of these events, however, depends more strongly on daily meteorological conditions and fuel continuity, in a context where fire suppression capacity is uneven and often limited in remote areas. This contrasts with Mediterranean systems, where highly effective suppression can dampen the influence of during-fire weather on final fire size.

4.3 Topography and landscape structure as primary controls of fire size

Random Forest (RF) models identified topographic, land cover (LC) and landscape-structure variables as the dominant predictors of final fire size in the Gran Chaco, with mean elevation, LC evenness, the tree–shrub–herb mosaic LC class and mean slope consistently ranking at the top of the SHAP-based hierarchy across all regional, seasonal and fire-weather configurations. The ordering remained stable in sensitivity experiments, and model performance declined when elevation and slope were removed (Fig. S20, Table S3), confirming that topography acts as an integrative proxy for geomorphological, hydrological and ecological gradients that shape the spatial context in which fires propagate. A mechanistic interpretation of vegetation effects in terms of fuel continuity and fuel moisture is developed in Sect. 4.4; this section focuses specifically on how elevation and slope structure the physical template of fire growth.

Elevation captures the major physiographic contrasts that structure fuel continuity across the Gran Chaco. In the Wet Chaco, extensive low-lying floodplains and seasonal wetlands generally limit fire spread but can become highly flammable during the dry season, especially following multi-year droughts when herbaceous biomass cures over broad, continuous surfaces. The marked increase in SHAP values below approximately 20–40 m reflects these drought-prone floodplain and marsh systems, where cured grasses form highly connected fuel beds that facilitate large fire growth. In contrast, slightly elevated terraces and woody islets (“montes” or “albardones”) interrupt fuel continuity and act as natural barriers that constrain lateral fire propagation. Spatial patterns in representative Wet Chaco landscapes (Figs. S21–S22) support this interpretation, with large fire patches consistently associated with drought-exposed, low-elevation herbaceous systems.

In the Dry Chaco, elevation contrasts distinguish floodplain matrices from agricultural mosaics and post-deforestation surfaces that break continuity. Here, the largest fires tend to occur on flat to gently elevated terrain where broad, relatively homogeneous landscape units maintain sufficiently connected fine fuels to support lateral fire growth. These tendencies align with landscape-level analyses in semi-arid central Argentina, where shrub-dominated fuel beds and topographically channeled winds promote the expansion of fire fronts (Fischer et al., 2012). In deforested landscapes, the spatial configuration of fuels is strongly

shaped by clearing patterns rather than by geomorphological gradients. As a result, BA within highly fragmented agricultural or recently cleared regions (Fig. S23) often exhibit weaker visual correspondence with elevation contrasts, since fuel continuity arises from land-use structure rather than from topographic controls.

In the Very Dry Chaco, rising elevation leads into sierran landscapes where open shrublands and xeric woodlands dominate. We found a near-linear positive association between fires and elevation up to several hundred meters, consistent with the concentration of large fires in shrub-dominated belts with continuous cured fuels along the mountains. Local examples from the Sierras de Córdoba (Fig. S23) demonstrate how topographic position aligns with vegetation structure. Similar relationships between physiographic position, shrub cover and extensive fire spread have been documented in other semi-arid regions of central Argentina (Fischer et al., 2012), underscoring that topography often serves as an effective proxy for the spatial organization of continuous fuels.

Slope provides complementary information to elevation. The largest fires overwhelmingly occur on surfaces with slopes below approximately 2 %–3 %, where lateral propagation is mostly unrestricted and drainage patterns do not fragment fuels. Steeper terrain consistently hosts smaller fires across the Wet and Dry Chaco, reflecting natural fuel discontinuities. In the Very Dry Chaco, most large fires also occur at low slopes, although some events exploit elongated ridge–valley structures at intermediate slopes, particularly in the sierran environments (Fig. S23). The combined behavior of elevation and slope explains why removing both variables in the sensitivity experiment substantially reduced model skill (Fig. S20).

Overall, these results indicate that topography structures the physical template within which fire growth unfolds, summarizing geomorphological and hydrological contrasts that influence where large, spatially connected burning conditions can develop. Although ignitions and land management are predominantly human-driven in the Gran Chaco, event-scale human-pressure proxies add limited incremental explanatory power once topography and landscape structure are accounted for; implications for fire use and land-use driven fuel restructuring are developed in Sect. 4.5.

4.4 Vegetation structure, fuel continuity and fuel moisture

Vegetation structure exerts a central influence on fire behavior in the Gran Chaco by shaping fuel continuity and the potential for lateral spread. Across the precipitation gradient, the largest fires occur in herbaceous and shrub-dominated systems where fine fuels can become continuous and seasonally flammable, whereas woody vegetation and heterogeneous mosaics constrain propagation (San Martín et al., 2023). These patterns align with long-standing ecological characterizations of Chaco fire regimes, in which open woodlands, grass–shrub mixtures and seasonally flooded herbaceous vegetation burn more extensively and more frequently than denser forest formations (Bravo et al., 2010, 2025; Naval-Fernández et al., 2025; San Martín et al., 2023; Vidal-Riveros et al., 2023). As discussed in Sect. 4.3, these vegetation effects operate within a topographic template, but they control fire growth primarily through the composition and spatial continuity of burnable fuels.

A key mechanism emerging from our results is the role of fuel continuity rather than fuel abundance per se. Herbaceous floodplain systems in the Wet Chaco and shrub-dominated systems in the Dry and Very Dry Chaco can provide highly connected fuel matrices during drought years, while woody islets, post-deforestation mosaics, cropland–grassland interfaces and other managed landscapes introduce sharp discontinuities that restrict spread. This mechanism is directly reflected in the strong importance of land cover evenness: low evenness (dominance by a single flammable class) is associated with large fires, whereas high evenness or high entropy corresponds to smaller events due to fragmentation. Similarly, the tree–shrub–herb mosaic class shows a strong negative influence, consistent with mixed woody patches acting as barriers and breaking connectivity.

These structure effects are also coherent with broader evidence that increasing tree cover often reduces burned area by limiting fine-fuel continuity and increasing shade and moisture retention (Bistinas et al., 2014; Haas et al., 2022). However, exceptions are well documented where particular forest types can be more flammable than native broadleaf formations, including introduced pine plantations in some regions (Barros and Pereira, 2014; Paritsis et al., 2018; Vidal-Riveros et al., 2023). In the Gran Chaco context, this underscores that "woody cover" is not a single fire-behavior category: the relevant control is how vegetation structure translates into horizontal continuity of ignitable fuels and seasonal drying.

A second dimension is fuel moisture seasonality, which varies markedly among growth forms. Experimental and remote-sensing work in the Southern Gran Chaco indicates that shrubs and grasses reach low live fuel moisture thresholds earlier in the dry season and maintain these conditions longer than tree species (Bianchi et al., 2014; Argañaraz et al., 2016, 2018). Differences in live fuel moisture among growth forms provide a mechanistic basis for the contrasting role of shrublands along the gradient, with shrub patches often limiting spread in wetter floodplain landscapes but promoting larger fires in drier regions where shrub matrices cure rapidly and sustain combustion over large areas. This is consistent with the broader finding that shrubs and grasses can reach lower moisture contents during the dry season than tree species (Yebra et al., 2019). Flooded herbaceous vegetation likewise can function either as a barrier or as a flammable matrix depending on hydrological conditions, becoming a major driver of large burns when multi-year droughts desiccate wetlands.

Productivity effects on fire behavior also emerge at broader temporal scales. We showed that vegetation greenness anomalies (EVI) respond tightly to antecedent rainfall and covary with FWI during the fire season, highlighting a classic fuel–productivity pathway: wet periods promote biomass accumulation, followed by curing during dry spells that increases flammability. This mechanism is widely documented in semi-arid Chaco systems (Bravo et al., 2010; Argañaraz et al., 2015; San Martín et al., 2023). In contrast, previous-season LAI, used here as a coarse proxy for accumulated biomass, played a comparatively minor role. LAI integrates total canopy foliage, including woody components, and therefore does not isolate the herbaceous and shrub layers most critical for fire spread. This likely explains its weak association with fire size in our models and reinforces the importance of considering fuel type and structure, rather than total leaf area, when interpreting vegetation controls on fire behavior in the Gran Chaco.

Taken together, these results show that vegetation structure mediates fire size in the Gran Chaco through three complementary mechanisms: (i) the fuel type and its degree of continuity across the landscape, which determines how far fires can propagate; (ii) the seasonal and interannual dynamics of fuel moisture, which vary among plant growth forms and strongly influence the timing and intensity of burning; and (iii) the productivity–curing sequence that links antecedent rainfall, herbaceous biomass accumulation and subsequent desiccation. These mechanisms operate differently along the precipitation–aridity gradient, producing distinct spatial fire regimes but a consistent overall pattern: large fires emerge primarily in continuous, fine-fuel systems that undergo strong seasonal drying, while fragmented or woody-dominated landscapes constrain spread regardless of weather conditions.

4.5 Human pressures and fire use in the Gran Chaco

Fire regimes worldwide are tightly linked to human activity: most ignitions are anthropogenic, and both land-use change and active suppression have reshaped BA patterns in many regions (Bowman et al., 2009, 2011; Archibald et al., 2013; Andela and van der Werf, 2014; Andela et al., 2017). The Gran Chaco fits within this global picture. It is a human-dominated dry forest and savanna system where fire is at once a natural ecological process and a widespread management tool, particularly in rangelands and agricultural frontiers (Bucher, 1982; Kunst and Bravo, 2003; Bravo et al., 2010, 2025).

Within the Gran Chaco, fire use is deeply embedded in pastoral and agricultural practices. Historical and ethnographic accounts document the use of fire by indigenous and rural communities in the Gran Chaco and neighboring ecoregions for hunting, communication, warfare and the management of plant resources (Arenas, 2003; Junk and Nunes da Cunha, 2012; Sugiyama et al., 2025). As in other tropical dry regions, most events are human-ignited and intentional, associated with land clearing, slash-and-burn deforestation or the disposal of residues, with a smaller fraction being accidental or natural (Baumann et al., 2018; De Marzo et al., 2023; Gasparri and Baldi, 2013; Gürtler, 2009). Modern land users routinely burn grasslands and savannas at the end of the dry season to stimulate grass regrowth and improve forage quality, often under informal or weakly regulated conditions (Kunst and Bravo, 2003; Kunst et al., 2016; Coronel et al., 2021; San Martín et al., 2023; Bravo et al., 2025). Many fires start in managed or unmanaged grasslands, savannas or croplands and subsequently spread into neighboring forests and shrublands (Bravo et al., 2010; Tálamo et al., 2013; Loto and Bravo, 2020; Giorgis et al., 2021; De Marzo et al., 2022). In this context, exotic grasses have been shown to enhance fuel continuity and fire intensity in several dryland systems (D'Antonio and Vitousek, 1992; Kunst et al., 2016; Bravo et al., 2025), but their spatial extent and dominance within the Gran Chaco remain heterogeneous and poorly constrained at regional scales. They should therefore be regarded as one of several possible mechanisms influencing fuel structure, rather than as a pervasive or dominant driver of large fires.

A further anthropogenic dimension concerns deforestation fires and the diverse forms of land-clearing burns that accompany agricultural expansion. In the Gran Chaco, the agricultural frontier has advanced rapidly over the past decades, and fire is routinely used to remove woody debris and prepare newly cleared fields, often as part of slash-and-burn cycles (Baumann et al., 2018, 2022; Boletta et al., 2006; De Marzo et al., 2023; Gasparri and Baldi, 2013; Gürtler, 2009). These fires can be extensive, but their spatial footprint depends strongly on how clearing interacts with fuel continuity, woody debris loads and local weather (San Martín et al., 2023).

A similar challenge applies to prescribed and semi-prescribed burns, which are widespread in rangeland management but rarely conducted under formal prescriptions or systematic monitoring frameworks (Bravo et al., 2025; Coria et al., 2021, p.202; Kunst et al., 2016; Kunst and Bravo, 2003). Many burns are intended to be low-intensity pasture treatments undertaken in late winter or early spring, yet under drought or wind anomalies they may escape control and evolve into landscape-scale events, as documented in multiple regions of the Gran Chaco. Although global inventories of prescribed fire exist (Hsu et al., 2025), they do not cover the Gran Chaco, underscoring the need for regional efforts to differentiate intentional, escaped and accidental fires. The lack of this information helps explain why our human-pressure variables account for little variance in final fire size: the signal of fire use is embedded within vegetation structure, fuel loads and land-cover mosaics, rather than through independent demographic metrics or ignition proxies that lack temporal and operational detail.

In this context, our finding that human-pressure variables play a secondary role in predicting final fire size does not

imply that humans are unimportant for the fire regime, but rather that their influence is mediated primarily through long-term land-use change and fuel restructuring. FRY v2.0 and related satellite products cannot distinguish between wildfires, escaped prescribed burns, deforestation fires or routine pasture burns, and thus the anthropogenic component enters the analysis mainly through its imprint on vegetation structure, land-cover mosaics and fuel continuity. As discussed in Sect. 4.1 and 4.4, the extreme fire seasons of 2019–2022 occurred during a prolonged La Niña episode that produced exceptional drought across the La Plata basin (Naumann et al., 2023; San Martín, 2024; Bravo et al., 2025). Despite changes in mobility and surveillance during the COVID-19 pandemic, large fires remained concentrated in fuel-rich, drought-stressed landscapes, indicating that climatic anomalies and fuel structure set the upper bound for fire size, while humans primarily determine ignition timing and location.

Livestock production offers a clear example of how human pressures modulate fire regimes indirectly. Grazing can interrupt the positive feedback between grasses and fire by reducing fine fuels, altering vegetation composition and promoting woody encroachment (Adámoli et al., 1990; Cingolani et al., 2013; Coria et al., 2021; Bravo et al., 2025). A global analysis showed that higher livestock densities in tropical rangelands are associated with lower fire frequency and increased shrub and dwarf tree cover (Bernardi et al., 2019), and regional syntheses for the Gran Chaco report that grazing interferes with fire–grass feedbacks and contributes to shrub expansion (Alessio et al., 2008; Alinari et al., 2015; Vidal-Riveros et al., 2023). The SHAP gradients we obtained for cattle density mirror these findings: large fires are concentrated at low to moderate densities, while high-density ranching landscapes are dominated by small events, consistent with a scenario where heavy grazing reduces continuous fine fuels and increases woody cover, thereby limiting maximum fire size even if fire weather remains conducive.

Road density and accessibility show a similar, albeit more complex, relationship. Numerous studies indicate that road expansion can both increase ignitions and fragment landscapes, thereby reducing the maximum size of individual fires (Andela and van der Werf, 2014; Bowring et al., 2024). In our analysis, both OpenStreetMap and Microsoft road detections density exhibited the same marginal pattern: large fires occur predominantly in areas with low road density, whereas regions with high road density are dominated by small fires. The sensitivity experiment substituting OSM with Microsoft roads confirmed that this pattern is robust and that differences in road datasets have negligible impact on predictive performance when medium to high resolution topography and LC mapping are included. The low overall importance of road density likely reflects two structural issues. First, road networks are strongly collinear with geography, LC composition and landscape heterogeneity, so much of their influence on fragmentation and suppression potential is already encoded by those variables. Second, averaging road density at the FP scale erases the spatial configuration of roads relative to ignition points and spread pathways, which is critical for understanding how roads constrain or redirect fire fronts.

Population density exhibits a comparable gradient, with sparse human presence associated with larger fires and densely populated areas dominated by smaller events, consistent with more active suppression, earlier detection and greater fuel management in productive landscapes. However, remotely sensed data and coarse demographic layers cannot capture the full social dimension of fire, including local perceptions, traditional burning practices and informal suppression. Recent reviews emphasize that the perspectives and knowledge of local communities are rarely incorporated into peer-reviewed fire research in the Gran Chaco, despite being widely discussed in grey literature and the media (McDaniel et al., 2005; Devisscher et al., 2016, 2019; Coronel et al., 2021; Vidal-Riveros et al., 2023). San Martín et al. (2023) and Bravo et al. (2025) explicitly call for interdisciplinary approaches that combine environmental and social sciences to better understand human–fire interactions in this region.

Overall, our results suggest that anthropogenic influences on fire size in the Gran Chaco operate mainly through their cumulative effects on vegetation structure, fuel continuity and landscape fragmentation, rather than through direct, independently measurable controls at the event scale. Ignitions are overwhelmingly human-driven, but the final size of fires is governed by the interaction between this ignition pressure, long-term land-use trajectories and the windows of opportunity created by drought and fire-conducive weather. Future work that integrates spatially explicit ignition records, fine-scale fuel management data, and socio-cultural information on fire use would allow a more complete quantification of the human contribution to fire size distributions in this rapidly changing dry forest biome. One good example of the potential of such interactions is presented in Hernández et al. (2022), who show that climate-related risks in rural Gran Chaco communities can only be understood through frameworks that combine environmental diagnostics with local practices, knowledge systems and power relations. Their coproduction process demonstrates that the way people perceive, monitor and respond to climatic hazards fundamentally shapes exposure and outcomes. A comparable socio-environmental approach applied to fire research could reveal how decisions about land clearing, burning, suppression and access interact with drought and fuel conditions to determine whether an ignition remains small or develops into a large fire.

4.6 Limitations and perspectives

Several limitations of this study stem from the nature of the available datasets and from methodological constraints. First, the meteorological information used to characterize fire weather, which relies on ERA5-Land at 0.1° resolu-

tion and cannot resolve local wind acceleration, channeled flows, shading, or fine-scale thermal gradients that influence fire spread in heterogeneous terrains. Although maximum wind speed and directional persistence emerged as meaningful predictors, the coarse resolution likely under-represents sub-kilometer variability in fire-atmosphere coupling, particularly in sierran environments. In addition, ERA5-Land precipitation is not bias-corrected, and its known tendency to smooth short-lived convective events at sub-daily scales may influence variables derived from it, such as total precipitation during the fire, potentially dampening the detection of sharp wetting or drying transitions within the time window of fire growth. Advances in downscaling techniques for wind (Dujardin and Lehning, 2022), solar radiation (Druel et al., 2025), and temperature (Kusch and Davy, 2022) may improve the spatial realism of these variables in future fire regime analyses, especially in complex landscapes. However, these approaches were not applied here.

Second, the FRY v2.0 dataset inherits all structural uncertainties of FireCCI51, including omission of small or low-intensity burns, overestimation in heterogeneous pixels, and potential inconsistencies in early MODIS years (Lizundia-Loiola et al., 2020; Pettinari et al., 2021). The reconstruction of FPs also depends on temporal grouping parameters that merge or split neighboring pixel clusters (Oom et al., 2016; Moreno et al., 2021). These issues constrain our ability to resolve very small events, the fine-scale geometry of scars, and rapid-fire spread fronts. The development of higher-resolution BA products has been repeatedly requested by the fire science community (Mouillot et al., 2014), and regional examples, such as the FireCCISFD20 product at 20 m for Africa (Chuvieco et al., 2022), have already demonstrated large gains in BA detection. Such advances will be essential to quantify fire size distributions and fire spread processes more accurately across the Gran Chaco.

Third, the satellite BA products used here do not provide information on fire type and therefore cannot distinguish among wildfires, escaped prescribed burns, deforestation fires, and routine rangeland burns. This restricts our capacity to attribute human-driven fire dynamics directly, since the anthropogenic signal enters the models primarily through long-term structural changes in vegetation composition, fragmentation and fuel continuity rather than through explicit information on ignition sources or operational decisions. The absence of spatially explicit ignition datasets, suppression records and fine-scale fuel management layers further limits our ability to separate environmental controls from management outcomes.

In the absence of direct information on fire type or ignition mechanism, human-pressure variables such as road density, population density or cattle density are used as indirect proxies for socio-environmental processes. Their weak importance in the RF models should therefore not be interpreted as evidence that human influence is negligible, but rather as a reflection of the limited thematic precision, spatial resolution and temporal representativeness of the available demographic and infrastructure datasets. These proxies capture only broad accessibility and land-use patterns, and they cannot represent operational decisions, intentional fire use or suppression capacity. As a result, landscape and LC variables at the scale of our analysis absorb much of the anthropogenic signal in our models.

Fourth, additional limitations arise from the interaction between the RF framework and the structure of the predictor datasets. Tree-based ensembles and SHAP-based rankings can be sensitive to differences in data quality, spatial support and collinearity among predictors. These conditions are better met by high-quality satellite-derived predictors such as elevation and annual land-cover layers than by demographic or infrastructure datasets, which are often coarser, noisier or less spatially complete. As a result, part of the dominant SHAP importance of topography and vegetation likely reflects both genuine structural controls on fuel continuity and the statistical advantages associated with these higher-quality predictors, rather than their purely mechanistic influence. The sensitivity experiment without topography confirms that elevation and slope summarize multiple unobserved gradients, partly compensating for limitations in other predictors. Although cross-validation diagnostics suggest limited overfitting, the RF remains bound to the chosen feature set and to the aggregation scale of fire patches. Future work could evaluate machine-learning architectures that operate directly on high-resolution imagery or spatial neighborhoods, for example through convolutional or graph-based neural networks combined with richer socio-economic layers, to test whether the predictor hierarchy found here is robust.

Fifth, several environmental variables used in this study should be interpreted as proxies rather than mechanistic drivers. Elevation and slope summarize hydrological, geomorphological and ecological gradients rather than exerting direct effects on combustion. Similarly, the previous-season LAI integrates productivity and vegetation structure but does not explicitly represent live fuel moisture or curing dynamics. Incorporating finer-resolution fuel moisture content datasets, daily vegetation optical depth or in situ biomass measurements (Argañaraz et al., 2016, 2018) would strengthen mechanistic interpretations.

Finally, our statistical models do not capture feedbacks between fire behavior and atmospheric processes, nor do they represent dynamic suppression, diurnal cycles of wind and humidity, or sub-daily fire-growth stages. Mechanistic fire-spread models and hybrid statistical–physical approaches could help resolve these processes and offer a complementary perspective.

Despite these limitations, our results provide a consistent regional picture: static landscape structure, summarized by topography and vegetation composition, dominates fire-size outcomes, while meteorology governs the windows of opportunity for rapid spread. Future work that combines high-resolution BA mapping, improved fire-weather fields, igni-

tion and management records, and socio-cultural dimensions of fire use would allow a more comprehensive understanding of the evolving fire regime of the Gran Chaco.

5 Conclusions

This study advances understanding of fire regimes across the Wet, Dry, and Very Dry Chaco through a spatially explicit analysis of fire events from 2001–2022. We document strong regional contrasts in fire size, seasonality and morphology, and show that these patterns arise from the combined effects of fuel structure, fire weather and long-term land use change.

Fire patch (FP) sizes were highly skewed: over 80 % of detected fires were $< 5\,km^2$, yet large events dominated total burned area (BA). Megafires ($> 100\,km^2$) occurred in all subregions, with the Wet Chaco recording the most. Gigafires ($> 1000\,km^2$) were rare but concentrated in the Dry Chaco, where some single events exceeded 50 % of annual BA. The Wet Chaco burned most extensively ($\sim 2\times$ the Dry Chaco), with the highest fire frequency and ignition density, reflecting greater biomass productivity and continuous fuels. The Very Dry Chaco, although it contributes the smallest share of total BA, is characterized by sporadic large, mega and gigafires that produce abrupt interannual peaks, consistent with a more stochastic fire regime where a few extreme events dominate variability.

The Fire Weather Index (FWI) displayed its strongest and most coherent relationship with BA and fire counts in the Wet Chaco, where most pixels (93 %) showed positive correlations between monthly FWI and BA anomalies (R up to 0.7), confirming a moisture limited regime. In the Dry and Very Dry Chaco, correlations were weaker and more heterogeneous, indicating that short term fire weather alone cannot explain spatial and interannual variability in BA. The extreme fire seasons of 2019–2022 coincided with a prolonged La Niña event and widespread positive FWI anomalies, especially in the Wet Chaco, yet some years with extensive burning occurred without exceptional FWI, underscoring the additional roles of fuel continuity, antecedent conditions and ignition patterns.

Lagged analyses revealed a fuel productivity mechanism in drier areas and a short-term drying control in wetter ones. In the Dry and Very Dry Chaco, positive rainfall and greenness anomalies several months before the fire season were followed by higher BA once fuels cured, consistent with a productivity–curing sequence where wet periods build biomass that later dries and burns. In wetter sectors of the Gran Chaco, shorter dry spells immediately before the fire season were more closely associated with BA peaks, reflecting conditions where fuels are rarely limiting and fire activity responds primarily to transient moisture deficits. La Niña phases strengthened fire potential across the region through reduced rainfall and elevated fire weather, and the clustering of extreme fire years at the end of the record suggests increasing exposure to such windows of opportunity.

Fire weather types (FWT) provided additional insight into how daily meteorology shapes fire outcomes. Pre-fire clustering captured ignition contexts but showed limited discrimination in final size or shape, consistent with a system where ignitions are predominantly anthropogenic and occur under broadly permissive conditions. In contrast, clustering based on during-fire meteorology separated neutral, drought-driven and wind-driven fires with clear differences in size and morphology. Wind-driven events were larger, more elongated and more cohesive than drought-driven fires, highlighting fire patch morphology as a signature of strong, persistent winds that could be used to benchmark process-based fire models and emerging machine learning approaches for fire behavior prediction.

Random Forest models showed that static landscape structure dominates fire size outcomes. Mean elevation, land cover evenness, a tree–shrub–herb mosaic land cover class and mean slope consistently ranked highest in SHAP based importance across regions, seasons and FWTs, ahead of meteorological and human pressure variables. With regional variations, large fires mostly concentrated in flat, low lying or gently elevated areas that host continuous herbaceous or shrub fuels, while steeper slopes and higher tree cover limited spread. Shrublands and flooded herbaceous vegetation played contrasted roles along the precipitation gradient, inhibiting spread in wetter, fragmented floodplains and supporting large fires in drier, shrub dominated matrices.

Human pressures in the Gran Chaco are essential for ignition but emerged as secondary for explaining the variation in final fire size once landscape structure is accounted for. Cattle, road, and population density all showed interpretable SHAP gradients, with larger fires occurring in remote, sparsely populated landscapes with low accessibility and low to moderate grazing pressure, and smaller fires in heavily managed areas with high road density or high stocking levels. However, their overall importance in the models was low, reflecting that most anthropogenic effects on fire size operate indirectly through long term transformations of vegetation structure, fuel continuity and fragmentation, or that they are hard to account for through remote sensing. Deforestation and land clearing fires contributed to BA, particularly in expanding agricultural frontiers, but the largest megafires and gigafires arose when continuous fine fuels, drought and wind aligned in ways that exceeded available suppression capacity.

By combining medium resolution FP data, reanalysis-based weather metrics, machine learning and landscape analysis, we identify key biophysical, climatic and anthropogenic determinants of fire size and shape in a major South American ecoregion, the Gran Chaco. Our results emphasize that topography and vegetation structure set the primary template for fire spread, that during-fire meteorology governs when ignited fires evolve into large, elongated events, and that hu-

man activities shape fire size mainly through their cumulative imprint on fuels and landscape configuration rather than through simple demographic gradients. These findings inform fire risk assessment and management under ongoing land use intensification and climate variability in the Gran Chaco, and highlight the need for high resolution BA products, improved fire weather fields, explicit ignition and management records and stronger integration of socio-cultural dimensions of fire use in order to anticipate how this fire regime will respond to future environmental and societal change.

Code and data availability. The fire-patch data used in this study were obtained from the FRYv2.0 database derived from FireCCI51 burned-area products (Laurent et al., 2018; Mouillot et al., 2023), available from the Open Science Framework repository at https://osf.io/rjvz5/files/osfstorage (last access: 10 June 2025). The underlying FireCCI51 burned-area product is described by Chuvieco et al. (2020) and Lizundia-Loiola et al. (2020). Meteorological variables were obtained from ERA5-Land via the Copernicus Climate Data Store (CDS) (Muñoz-Sabater et al., 2021; dataset DOI: https://doi.org/10.24381/cds.e2161bac, Muñoz Sabater, 2019), available at https://cds.climate.copernicus.eu/datasets/reanalysis-era5-land (last access: 30 May 2024). The Fire Weather Index calculations were initialized using Copernicus ERA5-FWI moisture codes at 0.25° (Vitolo et al., 2020). Calculations were performed with an adapted version of the FireDanger Python package, available at https://github.com/steidani/FireDanger (last access: 25 November 2025). Land-cover data were obtained from the ESA Climate Change Initiative Moderate Resolution Land Cover product available through the Copernicus Climate Data Store (dataset DOI: https://doi.org/10.24381/cds.006f2c9a, Copernicus Climate Change Service, Climate Data Store, 2019), at https://cds.climate.copernicus.eu/datasets/satellite-land-cover (last access: 26 May 2025), and described by Harper et al. (2023). Topographic data were obtained from the NASA SRTM v3 product at https://srtm.csi.cgiar.org (last access: 26 May 2025). River and lake layers used in Fig. 1 were obtained from HydroSHEDS (Lehner et al., 2008). MODIS leaf area index data were obtained from the MOD15A2H product for 2001–2002 and the MCD15A2H product for 2002–2023, available from NASA Earthdata (https://doi.org/10.5067/MODIS/MOD15A2H.061, Myeni et al., 2021a; https://doi.org/10.5067/MODIS/MCD15A2H.061, Myeni et al., 2021b). Soil variables, including soil organic carbon at 0–5 cm depth, sand fraction, and bulk density, were obtained from the SoilGrids250m database provided by ISRIC at https://data.isric.org (last access: 25 November 2025). Population density data were obtained from the Gridded Population of the World, Version 4 (GPWv4): Population Density, Revision 11 dataset (Center for International Earth Science Information Network (CIESIN), 2017, https://doi.org/10.7927/H49C6VHW), available at https://www.earthdata.nasa.gov/data/projects/gpw (last access: 25 November 2025). Livestock density data were obtained from the Gridded Livestock of the World version 4 (GLWv4), available from Harvard Dataverse at https://dataverse.harvard.edu/dataverse/glw_4 (last access: 25 November 2025). Road data were obtained from OpenStreetMap at https://www.openstreetmap.org and from the Microsoft Global Roads dataset at https://github.com/microsoft/RoadDetections (last access: 25 November 2025 for both). The Multivariate ENSO Index version 2 (MEI.v2) was obtained from the NOAA Physical Sciences Laboratory at https://psl.noaa.gov/enso/mei/ (last access: 26 May 2025). The scripts used for data processing, statistical analysis, and figure generation were developed by the authors and are available from the corresponding author upon reasonable request.

Supplement. The supplement related to this article is available online at https://doi.org/10.5194/nhess-26-1479-2026-supplement.

Author contributions. RSM collected and processed the data, analyzed the results, and drafted the manuscript. CO and AS conceived the idea and led the project. PVA contributed to data analysis, specifically by performing Random Forest modeling. All co-authors discussed the results, provided critical feedback, and reviewed the manuscript.

Competing interests. The contact author has declared that none of the authors has any competing interests.

Disclaimer. Publisher's note: Copernicus Publications remains neutral with regard to jurisdictional claims made in the text, published maps, institutional affiliations, or any other geographical representation in this paper. The authors bear the ultimate responsibility for providing appropriate place names. Views expressed in the text are those of the authors and do not necessarily reflect the views of the publisher.

Acknowledgements. The authors thank all the researchers and institutions involved in providing open-access datasets, including ESA CCI, ERA5-Land, and the Copernicus Climate Data Store (CDS). We acknowledge the computational infrastructure and support provided by the Laboratoire des Sciences du Climat et de l'Environnement (LSCE/IPSL). We also express our gratitude to Dr. Sandra Bravo for her important collaboration and contributions to our understanding of the fire regime in the region, as well as colleagues from CONICET for their valuable insights into Chaco ecology. We would like to thank the two anonymous reviewers for their valuable comments and suggestions, which helped us to improve the quality of the manuscript. The authors also acknowledge the use of AI-based tools to assist with text editing, code debugging, and figure scripting throughout the preparation of the manuscript.

Financial support. This research was partially funded by the European Space Agency through the Climate Change Initiative programme, under contract numbers ESA/No. 4000126564 (CCI MRLC) and ESA ESRIN/No. 4000125259/18/I-NB (CCI HRLC). R. San Martin received doctoral funding from the Environmental Science Doctoral School of Île-de-France (DS 129). A. Sörensson acknowledges support from the Agencia Nacional de Promo-

ción Científica y Tecnológica (ANPCyT, Argentina) via project PICT 2018-02511, and from the Consejo Nacional de Investigaciones Científicas y Técnicas (CONICET, Argentina) through grant PIP 11220200102141CO. F. Mouillot acknowledges support from the ESA FireCCI project (Contract No. 4000126706/19/I-NB), and from the FIRE-ADAPT project (EU grant HORIZON-MSCA-2021-SE-01086416).

Review statement. This paper was edited by Ugur Öztürk and reviewed by two anonymous referees.

References

Adámoli, J., Sennhauser, E., Acero, J. M., and Rescia, A.: Stress and Disturbance: Vegetation Dynamics in the Dry Chaco Region of Argentina, J. Biogeogr., 17, 491–500, https://doi.org/10.2307/2845381, 1990.

Alencar, A. A., Brando, P. M., Asner, G. P., and Putz, F. E.: Landscape fragmentation, severe drought, and the new Amazon forest fire regime, Ecol. Appl., 25, 1493–1505, https://doi.org/10.1890/14-1528.1, 2015.

Alessio, G. A., Peñuelas, J., Llusià, J., Ogaya, R., Estiarte, M., and De Lillis, M.: Influence of water and terpenes on flammability in some dominant Mediterranean species, Int. J. Wildland Fire, 17, 274–286, https://doi.org/10.1071/WF07038, 2008.

Alinari, J., von Muller, A., and Renison, D.: The contribution of fire damage to restricting high mountain Polylepis australis forests to ravines: Insights from an un-replicated comparison, Ecología Austral., 25, 11–18, https://doi.org/10.25260/EA.15.25.1.0.53, 2015.

Andela, N. and van der Werf, G. R.: Recent trends in African fires driven by cropland expansion and El Niño to La Niña transition, Nat. Clim. Change, 4, 791–795, https://doi.org/10.1038/nclimate2313, 2014.

Andela, N., Morton, D. C., Giglio, L., Chen, Y., van der Werf, G. R., Kasibhatla, P. S., DeFries, R. S., Collatz, G. J., Hantson, S., Kloster, S., Bachelet, D., Forrest, M., Lasslop, G., Li, F., Mangeon, S., Melton, J. R., Yue, C., and Randerson, J. T.: A human-driven decline in global burned area, Science, 356, 1356–1362, https://doi.org/10.1126/science.aal4108, 2017.

Andela, N., Morton, D. C., Giglio, L., Paugam, R., Chen, Y., Hantson, S., van der Werf, G. R., and Randerson, J. T.: The Global Fire Atlas of individual fire size, duration, speed and direction, Earth Syst. Sci. Data, 11, 529–552, https://doi.org/10.5194/essd-11-529-2019, 2019.

Archibald, S., Roy, D. P., Van WILGEN, B. W., and Scholes, R. J.: What limits fire? An examination of drivers of burnt area in Southern Africa, Glob. Change Biol., 15, 613–630, https://doi.org/10.1111/j.1365-2486.2008.01754.x, 2009.

Archibald, S., Lehmann, C. E. R., Gómez-Dans, J. L., and Bradstock, R. A.: Defining pyromes and global syndromes of fire regimes, P. Natl. Acad. Sci. USA, 110, 6442–6447, https://doi.org/10.1073/pnas.1211466110, 2013.

Archibald, S., Lehmann, C. E. R., Belcher, C. M., Bond, W. J., Bradstock, R. A., Daniau, A.-L., Dexter, K. G., Forrestel, E. J., Greve, M., He, T., Higgins, S. I., Hoffmann, W. A., Lamont, B. B., McGlinn, D. J., Moncrieff, G. R., Osborne, C. P., Pausas, J. G., Price, O., Ripley, B. S., Rogers, B. M., Schwilk, D. W., Simon, M. F., Turetsky, M. R., Van der Werf, G. R., and Zanne, A. E.: Biological and geophysical feedbacks with fire in the Earth system, Environ. Res. Lett., 13, 033003, https://doi.org/10.1088/1748-9326/aa9ead, 2018.

Arenas, P.: ARENAS, Pastor, Etnografía y alimentación entre los toba-ñachilamole#ek y wichí-lhuku'tas del Chaco Central (Argentina), Buenos Aires, Edición del autor, 562 p., ISBN 987-43-6483-1, 2003.

Argañaraz, Pizarro, G. G., Zak, M., Landi, M. A., and Bellis, L. M.: Human and biophysical drivers of fires in Semiarid Chaco mountains of Central Argentina, Sci. Total Environ., 520, 1–12, https://doi.org/10.1016/j.scitotenv.2015.02.081, 2015.

Argañaraz, Landi, M. A., Bravo, S. J., Gavier-Pizarro, G. I., Scavuzzo, C. M., and Bellis, L. M.: Estimation of Live Fuel Moisture Content From MODIS Images for Fire Danger Assessment in Southern Gran Chaco, IEEE J. Sel. Top. Appl. Earth Obs., 9, 5339–5349, https://doi.org/10.1109/JSTARS.2016.2575366, 2016.

Argañaraz, Landi, M. A., Scavuzzo, C. M., and Bellis, L. M.: Determining fuel moisture thresholds to assess wildfire hazard: A contribution to an operational early warning system, PLoS ONE, 13, e0204889, https://doi.org/10.1371/journal.pone.0204889, 2018.

Arias, P. A., Rivera, J. A., Sörensson, A. A., Zachariah, M., Barnes, C., Philip, S., Kew, S., Vautard, R., Koren, G., Pinto, I., Vahlberg, M., Singh, R., Raju, E., Li, S., Yang, W., Vecchi, G. A., and Otto, F. E. L.: Interplay between climate change and climate variability: the 2022 drought in Central South America, Climatic Change, 177, https://doi.org/10.1007/s10584-023-03664-4, 2024.

Barros, A. M. G. and Pereira, J. M. C.: Wildfire Selectivity for Land Cover Type: Does Size Matter?, PLOS ONE, 9, e84760, https://doi.org/10.1371/journal.pone.0084760, 2014.

Barros, V., Clarke, R., and Silva Dias, P.: Climate Change in the La Plata Basin, Inter-American Institute for Global Change Research (IAI), São José dos Campos, Brazil, http://www-atmo.at.fcen.uba.ar/cordex/Barrosetal2006ChapterII.pdf (last access: 10 March 2026), 2006.

Baumann, M., Levers, C., Macchi, L., Bluhm, H., Waske, B., Gasparri, N. I., and Kuemmerle, T.: Mapping continuous fields of tree and shrub cover across the Gran Chaco using Landsat 8 and Sentinel-1 data, Remote Sens. Environ., 216, 201–211, https://doi.org/10.1016/j.rse.2018.06.044, 2018.

Baumann, M., Gasparri, I., Buchadas, A., Oeser, J., Meyfroidt, P., Levers, C., Romero-Muñoz, A., le Polain de Waroux, Y., Müller, D., and Kuemmerle, T.: Frontier metrics for a process-based understanding of deforestation dynamics, Environ. Res. Lett., 17, 095010, https://doi.org/10.1088/1748-9326/ac8b9a, 2022.

Belhadj-Khedher, C., El-Melki, T., and Mouillot, F.: Saharan Hot and Dry Sirocco Winds Drive Extreme Fire Events in Mediterranean Tunisia (North Africa), Atmosphere, 11, 590, https://doi.org/10.3390/atmos11060590, 2020.

Bernardi, R. E., Staal, A., Xu, C., Scheffer, M., and Holmgren, M.: Livestock Herbivory Shapes Fire Regimes and Vegetation Structure Across the Global Tropics, Ecosystems, 22, 1457–1465, https://doi.org/10.1007/s10021-019-00349-x, 2019.

Bianchi, L., Defossé, G., Dentoni, M., Kunst, C., Ledesma, R., and Bravo, S.: Dynamics of fuel moisture and its relation to the ecology and management of fire in the western Chaco region

(Argentina) I: basic concepts, IA – Revista de Investigaciones Agropecuarias, 40, 154–164, 2014.

Bistinas, I., Harrison, S. P., Prentice, I. C., and Pereira, J. M. C.: Causal relationships versus emergent patterns in the global controls of fire frequency, Biogeosciences, 11, 5087–5101, https://doi.org/10.5194/bg-11-5087-2014, 2014.

Boletta, P. E., Ravelo, A. C., Planchuelo, A. M., and Grilli, M.: Assessing deforestation in the Argentine Chaco, Forest Ecol. Manag., 228, 108–114, https://doi.org/10.1016/j.foreco.2006.02.045, 2006.

Bowman, Balch, J., Artaxo, P., Bond, W. J., Cochrane, M. A., D'Antonio, C. M., DeFries, R., Johnston, F. H., Keeley, J. E., Krawchuk, M. A., Kull, C. A., Mack, M., Moritz, M. A., Pyne, S., Roos, C. I., Scott, A. C., Sodhi, N. S., and Swetnam, T. W.: The human dimension of fire regimes on Earth: The human dimension of fire regimes on Earth, J. Biogeogr., 38, 2223–2236, https://doi.org/10.1111/j.1365-2699.2011.02595.x, 2011.

Bowman, D. M. J. S., Balch, J. K., Artaxo, P., Bond, W. J., Carlson, J. M., Cochrane, M. A., D'Antonio, C. M., DeFries, R. S., Doyle, J. C., Harrison, S. P., Johnston, F. H., Keeley, J. E., Krawchuk, M. A., Kull, C. A., Marston, J. B., Moritz, M. A., Prentice, I. C., Roos, C. I., Scott, A. C., Swetnam, T. W., van der Werf, G. R., and Pyne, S. J.: Fire in the Earth System, Science, 324, 481–484, https://doi.org/10.1126/science.1163886, 2009.

Bowring, S. P. K., Li, W., Mouillot, F., Rosan, T. M., and Ciais, P.: Road fragment edges enhance wildfire incidence and intensity, while suppressing global burned area, Nat. Commun., 15, 9176, https://doi.org/10.1038/s41467-024-53460-6, 2024.

Bravo, S., Kunst, C., Grau, R., and Aráoz, E.: Fire–rainfall relationships in Argentine Chaco savannas, J. Arid Environ., 74, 1319–1323, https://doi.org/10.1016/j.jaridenv.2010.04.010, 2010.

Bravo, S., Kunst, C., Leiva, M., and Ledesma, R.: Response of hardwood tree regeneration to surface fires, western Chaco region, Argentina, Forest Ecol. Manag., 326, 36–45, https://doi.org/10.1016/j.foreco.2014.04.009, 2014.

Bravo, S., Bogino, S., Leiva, M., Lepiscopo, M., Cendoya, M., Kunst, C., and Biurrun, F.: Wood anatomy, fire wounds and dendrochronological potential of Prosopis pugionata Burkart (Fabaceae) in arid Argentine Chaco, IAWA J., 42, 1–10, https://doi.org/10.1163/22941932-bja10056, 2021.

Bravo, S., Ledesma, R., Coria, D., and Loto, D.: Fire in the Chaco Region: Ecological Aspects and Land Management, in: Fire in the South American Ecosystems, edited by: Fidelis, A. and Pivello, V. R., Springer Nature Switzerland, Cham, 213–241, https://doi.org/10.1007/978-3-031-89372-8_8, 2025.

Bucher, E. H.: Chaco and Caatinga – South American Arid Savannas, Woodlands and Thickets, in: Ecology of Tropical Savannas, vol. 42, edited by: Huntley, B. J. and Walker, B. H., Springer Berlin Heidelberg, Berlin, Heidelberg, 48–79, https://doi.org/10.1007/978-3-642-68786-0_4, 1982.

Bucher, E. H. and Huszar, P. C.: Sustainable management of the Gran Chaco of South America: Ecological promise and economic constraints, J. Environ. Manage., 57, 99–108, https://doi.org/10.1006/jema.1999.0290, 1999.

Cabrera, A.: Regiones fitogeo-gráficas argentina, Enciclopedia Argentina de Agricultura y Jardinería, 2, https://www.sidalc.net/search/Record/KOHA-OAI-FCF:2863/Description (last access: 10 March 2026), 1976.

Castilla, M.: " Ahora tenemos este virus, pero cuando tenés tantos problemas en la zona nada alcanza": Extractivismo, segregación y pandemia en la provincia del Chaco, Quid 16 – Revista del Área de Estudios Urbanos, 16, 8–38, https://dialnet.unirioja.es/servlet/articulo?codigo=8239107 (last access: 10 March 2026), 2021.

Center For International Earth Science Information Network (CIESIN) Columbia University: Gridded Population of the World, Version 4 (GPWv4): Population Density, Revision 11, Palisades, NY: NASA Socioeconomic Data and Applications Center (SEDAC) [data set], https://doi.org/10.7927/H49C6VHW, 2017.

Chuvieco, E., Aguado, I., Salas, J., García, M., Yebra, M., and Oliva, P.: Satellite Remote Sensing Contributions to Wildland Fire Science and Management, Curr. Forestry Rep., 6, 81–96, https://doi.org/10.1007/s40725-020-00116-5, 2020.

Chuvieco, E., Roteta, E., Sali, M., Stroppiana, D., Boettcher, M., Kirches, G., Storm, T., Khairoun, A., Pettinari, M. L., Franquesa, M., and Albergel, C.: Building a small fire database for Sub-Saharan Africa from Sentinel-2 high-resolution images, Sci. Total Environ., 845, 157139, https://doi.org/10.1016/j.scitotenv.2022.157139, 2022.

Cingolani, A. M., Vaieretti, M. V., Giorgis, M. A., La Torre, N., Whitworth-Hulse, J. I., and Renison, D.: Can livestock and fires convert the sub-tropical mountain rangelands of central Argentina into a rocky desert?, Rangel J., 35, 285–297, https://doi.org/10.1071/RJ12095, 2013.

Coria, R. D., Kunst, C. R., and Bravo, S. J.: A contribution to the understanding of the woody encroachment in grasslands/savannas from the South American Semiarid Chaco, Ecol. Austral., 31, 595–607, https://doi.org/10.25260/EA.21.31.3.0.1615, 2021.

Copernicus Climate Change Service, Climate Data Store: Land cover classification gridded maps from 1992 to present derived from satellite observation, Copernicus Climate Change Service (C3S) Climate Data Store (CDS) [data set], https://doi.org/10.24381/cds.006f2c9a, 2019.

Coronel, G., Pastén, M., Breuer, N., Celeste, A., Rejalaga, L., Domecq, F. M., and Nagy, G. J.: Wildfires in Paraguay: Environmental and Human Impacts, in: Sustainability in Natural Resources Management and Land Planning, edited by: Leal Filho, W., Azeiteiro, U. M., and Setti, A. F. F., Springer International Publishing, Cham, 429–444, https://link.springer.com/chapter/10.1007/978-3-030-76624-5_25 (last access: 13 March 2026), 2021.

D'Antonio, C. M. and Vitousek, P. M.: Biological Invasions by Exotic Grasses, the Grass/Fire Cycle, and Global Change, Annu. Rev. Ecol. Syst., 23, 63–87, 1992.

De Marzo, T., Pflugmacher, D., Baumann, M., Lambin, E. F., Gasparri, I., and Kuemmerle, T.: Characterizing forest disturbances across the Argentine Dry Chaco based on Landsat time series, Int. J. Appl. Earth Obs., 98, 102310, https://doi.org/10.1016/j.jag.2021.102310, 2021.

De Marzo, T., Gasparri, N. I., Lambin, E. F., and Kuemmerle, T.: Agents of Forest Disturbance in the Argentine Dry Chaco, Remote Sens., 14, 1758, https://doi.org/10.3390/rs14071758, 2022.

De Marzo, T., Pratzer, M., Baumann, M., Gasparri, N. I., Pötzschner, F., and Kuemmerle, T.: Linking disturbance history to current forest structure to assess the impact of distur-

bances in tropical dry forests, Forest Ecol. Manag., 539, 120989, https://doi.org/10.1016/j.foreco.2023.120989, 2023.

Defourny, P., Lamarche, C., Brockmann, C., Boettcher, M., Bontemps, S., Maet, T., Duveiller, G., Kirches, G., Moreau, I., Peylin, P., Ottlé, C., Ramoino, F., Bogaert, E., Albergel, C., and Arino, O.: Observed annual global land-use change from 1992 to 2020 three times more dynamic than reported by inventory-based statistics, in preparation, 2023.

Devisscher, T., Boyd, E., and Malhi, Y.: Anticipating future risk in social-ecological systems using fuzzy cognitive mapping: the case of wildfire in the Chiquitania, Bolivia, Ecol. Soc., 21, https://doi.org/10.5751/ES-08599-210418, 2016.

Devisscher, T., Malhi, Y., and Boyd, E.: Deliberation for wildfire risk management: Addressing conflicting views in the Chiquitania, Bolivia, Geogr. J., 185, 38–54, https://doi.org/10.1111/geoj.12261, 2019.

Doblas-Reyes, F. J., Sörensson, A. A., Almazroui, M., Dosio, A., Gutowski, W. J., Haarsma, R., Hamdi, R., Hewitson, B., Kwon, W.-T., Lamptey, B. L., Maraun, D., Stephenson, T. S., Takayabu, I., Terray, L., Turner, A., and Zuo, Z.: Linking global to regional climate change, in: Climate Change 2021: The Physical Science Basis, Contribution of Working Group I to the Sixth Assessment Report of the Intergovernmental Panel on Climate Change, edited by: Masson-Delmotte, V., Zhai, P., Pirani, A., Connors, S. L., Péan, C., Berger, S., Caud, N., Chen, Y., Goldfarb, L., Gomis, M. I., Huang, M., Leitzell, K., Lonnoy, E., Matthews, J. B. R., Maycock, T. K., Waterfield, T., Yelekçi, O., Yu, R., and Zhou, B., Cambridge University Press, Cambridge, UK and New York, NY, USA, 1363–1512, https://doi.org/10.1017/9781009157896.012, 2021.

Druel, A., Ruffault, J., Davi, H., Chanzy, A., Marloie, O., De Cáceres, M., Olioso, A., Mouillot, F., François, C., Soudani, K., and Martin-StPaul, N. K.: Enhancing environmental models with a new downscaling method for global radiation in complex terrain, Biogeosciences, 22, 1–18, https://doi.org/10.5194/bg-22-1-2025, 2025.

Dujardin, J. and Lehning, M.: Wind-Topo: Downscaling near-surface wind fields to high-resolution topography in highly complex terrain with deep learning, Q. J. Roy. Meteor. Soc., 148, 1368–1388, https://doi.org/10.1002/qj.4265, 2022.

Eklund, J., Jones, J. P. G., Räsänen, M., Geldmann, J., Jokinen, A.-P., Pellegrini, A., Rakotobe, D., Rakotonarivo, O. S., Toivonen, T., and Balmford, A.: Elevated fires during COVID-19 lockdown and the vulnerability of protected areas, Nat. Sustain., 5, 603–609, https://doi.org/10.1038/s41893-022-00884-x, 2022.

Feron, S., Cordero, R. R., Damiani, A., MacDonell, S., Pizarro, J., Goubanova, K., Valenzuela, R., Wang, C., Rester, L., and Beaulieu, A.: South America is becoming warmer, drier, and more flammable, Commun. Earth Environ., 5, https://doi.org/10.1038/s43247-024-01654-7, 2024.

Fischer, M. A., Di Bella, C. M., and Jobbágy, E. G.: Fire patterns in central semiarid Argentina, J. Arid Environ., 78, 161–168, https://doi.org/10.1016/j.jaridenv.2011.11.009, 2012.

Garcia, L. C., Szabo, J. K., de Oliveira Roque, F., de Matos Martins Pereira, A., Nunes da Cunha, C., Damasceno-Júnior, G. A., Morato, R. G., Tomas, W. M., Libonati, R., and Ribeiro, D. B.: Record-breaking wildfires in the world's largest continuous tropical wetland: Integrative fire management is urgently needed for both biodiversity and humans, J. Environ. Manage., 293, 112870, https://doi.org/10.1016/j.jenvman.2021.112870, 2021.

García, M., Pettinari, M. L., Chuvieco, E., Salas, J., Mouillot, F., Chen, W., and Aguado, I.: Characterizing Global Fire Regimes from Satellite-Derived Products, Forests, 13, 699, https://doi.org/10.3390/f13050699, 2022.

Gasparri, N. I. and Baldi, G.: Regional patterns and controls of biomass in semiarid woodlands: lessons from the Northern Argentina Dry Chaco, Reg. Environ. Change, 13, 1131–1144, https://doi.org/10.1007/s10113-013-0422-x, 2013.

Gasparri, N. I., Grau, H. R., and Manghi, E.: Carbon Pools and Emissions from Deforestation in Extra-Tropical Forests of Northern Argentina Between 1900 and 2005, Ecosystems, 11, 1247–1261, https://doi.org/10.1007/s10021-008-9190-8, 2008.

Ginzburg, R., Adámoli, J., Herrera, P., and Torrella, S.: Los Humedales del Chaco: clasificación, inventario y mapeo a escala regional, Miscelánea, 14, 121–138, 2005.

Giorgis, M. A., Zeballos, S. R., Carbone, L., Zimmermann, H., von Wehrden, H., Aguilar, R., Ferreras, A. E., Tecco, P. A., Kowaljow, E., Barri, F., Gurvich, D. E., Villagra, P., and Jaureguiberry, P.: A review of fire effects across South American ecosystems: the role of climate and time since fire, Fire Ecol., 17, https://doi.org/10.1186/s42408-021-00100-9, 2021.

Gürtler, R. E.: Sustainability of vector control strategies in the Gran Chaco Region: current challenges and possible approaches, Memórias do Instituto Oswaldo Cruz, 104, 52–59, 2009.

Haas, O., Prentice, I. C., and Harrison, S. P.: Global environmental controls on wildfire burnt area, size, and intensity, Environ. Res. Lett., 17, 065004, https://doi.org/10.1088/1748-9326/ac6a69, 2022.

Hantson, S., Pueyo, S., and Chuvieco, E.: Global fire size distribution is driven by human impact and climate, Global Ecol. Biogeogr., 24, 77–86, https://doi.org/10.1111/geb.12246, 2015.

Hantson, S., Scheffer, M., Pueyo, S., Xu, C., Lasslop, G., Nes, E. H., and Mendelsohn, J.: Rare, Intense, Big fires dominate the global tropics under drier conditions, Sci. Rep., 7, 1–5, 2017.

Harper, K. L., Lamarche, C., Hartley, A., Peylin, P., Ottlé, C., Bastrikov, V., San Martín, R., Bohnenstengel, S. I., Kirches, G., Boettcher, M., Shevchuk, R., Brockmann, C., and Defourny, P.: A 29-year time series of annual 300 m resolution plant-functional-type maps for climate models, Earth Syst. Sci. Data, 15, 1465–1499, https://doi.org/10.5194/essd-15-1465-2023, 2023.

Hernandez, C., Drobinski, P., and Turquety, S.: How much does weather control fire size and intensity in the Mediterranean region?, Ann. Geophys., 33, 931–939, https://doi.org/10.5194/angeo-33-931-2015, 2015.

Hernández, V., Florencia Fossa Riglos, M., and Vera, C.: Addressing climate services in SouthAmerican Chaco region through a knowledge coproduction process, Global Environ. Chang., 72, 102443, https://doi.org/10.1016/j.gloenvcha.2021.102443, 2022.

Higuera, P. E., Abatzoglou, J. T., Littell, J. S., and Morgan, P.: The Changing Strength and Nature of Fire-Climate Relationships in the Northern Rocky Mountains, U.S.A., 1902–2008, PLOS ONE, 10, e0127563, https://doi.org/10.1371/journal.pone.0127563, 2015.

Horn, B. K. P.: Hill shading and the reflectance map, P. IEEE, 69, 14–47, https://doi.org/10.1109/PROC.1981.11918, 1981.

Hsu, A., Jones, M. W., Thurgood, J. R., Smith, A. J. P., Carmenta, R., Abatzoglou, J. T., Anderson, L. O., Clarke, H., Doerr, S.

H., Fernandes, P. M., Kolden, C. A., Santín, C., Strydom, T., Le Quéré, C., Ascoli, D., Castellnou, M., Goldammer, J. G., Guiomar, N. R. G. N., Kukavskaya, E. A., Rigolot, E., Tanpipat, V., Varner, M., Yamashita, Y., Baard, J., Barreto, R., Becerra, J., Brunn, E., Bergius, N., Carlsson, J., Cheney, C., Druce, D., Elliot, A., Evans, J., De Moraes Falleiro, R., Prat-Guitart, N., Hiers, J. K., Kaiser, J. W., Macher, L., Morris, D., Park, J., Robles, C., Román-Cuesta, R. M., Rücker, G., Senra, F., Steil, L., Valverde, J. A. L., and Zerr, E.: A global assemblage of regional prescribed burn records – GlobalRx, Sci. Data, 12, 1083, https://doi.org/10.1038/s41597-025-04941-w, 2025.

Jones, Abatzoglou, J. T., Veraverbeke, S., Andela, N., Lasslop, G., and Forkel, M.: Global and regional trends and drivers of fire under climate change, Rev. Geophys., 60, e2020RG000726, https://doi.org/10.1029/2020RG000726, 2022.

Junk, W. J. and Nunes da Cunha, C.: Pasture clearing from invasive woody plants in the Pantanal: a tool for sustainable management or environmental destruction?, Wetl. Ecol. Manag., 20, 111–122, https://doi.org/10.1007/s11273-011-9246-y, 2012.

Kelley, D. I., Bistinas, I., Whitley, R., Burton, C., Marthews, T. R., and Dong, N.: How contemporary bioclimatic and human controls change global fire regimes, Nat. Clim. Change, 9, 690–696, https://doi.org/10.1038/s41558-019-0540-7, 2019.

Krawchuk, M. A. and Moritz, M. A.: Constraints on global fire activity vary across a resource gradient, Ecology, 92, 121–132, https://doi.org/10.1890/09-1843.1, 2011.

Kumar, S., Getirana, A., Libonati, R., Hain, C., Mahanama, S., and Andela, N.: Changes in land use enhance the sensitivity of tropical ecosystems to fire-climate extremes, Sci. Rep., 12, 964, https://doi.org/10.1038/s41598-022-05130-0, 2022.

Kunst, C. and Bravo, S.: Ecología y régimen de fuego en la región chaqueña argentina, in: Fuego en los ecosistemas argentinos, edited by: Kunst, C., Bravo, S., and Panigatti, J. L., Ediciones INTA, Buenos Aires, 109–118, 2003.

Kunst, C., Bravo, S., Monti, E., Cornacchione, M., and Godoy, J.: El fuego y el manejo de pasturas naturales y cultivadas de la región chaqueña, Fuego en los Ecosistemas Argentinos, Ediciones INTA, 21, 239–247, 2003.

Kunst, C., Navall, M., Ledesma, R., Silberman, J., Anríquez, A., Coria, D., Bravo, S., Gómez, A., Albanesi, A., Grasso, D., Nuñez, J. A. D., González, A., Tomsic, P., and Godoy, J.: Silvopastoral Systems in the Western Chaco Region, Argentina, in: Silvopastoral Systems in Southern South America, edited by: Peri, P. L., Dube, F., and Varella, A., Springer International Publishing, Cham, 63–87, https://doi.org/10.1007/978-3-319-24109-8_4, 2016.

Kusch, E. and Davy, R.: KrigR – A tool for downloading and statistically downscaling climate reanalysis data, Environ. Res. Lett., 17, https://doi.org/10.1088/1748-9326/ac48b3, 2022.

Laurent, P., Mouillot, F., Yue, C., Ciais, P., Moreno, M. V., and Nogueira, J. M. P.: FRY, a global database of fire patch functional traits derived from space-borne burned area products, Sci. Data, 5, 180132, https://doi.org/10.1038/sdata.2018.132, 2018.

Lehner, B., Verdin, K., and Jarvis, A.: New global hydrography derived from spaceborne elevation data, Eos, Transactions American Geophysical Union, 89, 93–94, 2008.

Levers, C., Piquer-Rodríguez, M., Gollnow, F., Baumann, M., Camino, M., Gasparri, N. I., Gavier-Pizarro, G. I., le Polain de Waroux, Y., Müller, D., Nori, J., Pötzschner, F., Romero-Muñoz, A., and Kuemmerle, T.: What is still at stake in the Gran Chaco? Social-ecological impacts of alternative land-system futures in a global deforestation hotspot, Environ. Res. Lett., 19, 064003, https://doi.org/10.1088/1748-9326/ad44b6, 2024.

Linley, G. D., Jolly, C. J., Doherty, T. S., Geary, W. L., Armenteras, D., Belcher, C. M., Bliege Bird, R., Duane, A., Fletcher, M., Giorgis, M. A., Haslem, A., Jones, G. M., Kelly, L. T., Lee, C. K. F., Nolan, R. H., Parr, C. L., Pausas, J. G., Price, J. N., Regos, A., Ritchie, E. G., Ruffault, J., Williamson, G. J., Wu, Q., and Nimmo, D. G.: What do you mean, 'megafire'?, Global Ecol. Biogeogr., 31, 1906–1922, https://doi.org/10.1111/geb.13499, 2022.

Lizundia-Loiola, J., Otón, G., Ramo, R., and Chuvieco, E.: A spatio-temporal active-fire clustering approach for global burned area mapping at 250 m from MODIS data, Remote Sens. Environ., 236, 111493, https://doi.org/10.1016/j.rse.2019.111493, 2020.

Loto, D. and Bravo, S.: Species composition, structure, and functional traits in Argentine Chaco forests under two different disturbance histories, Ecol. Indic., 113, 106232, https://doi.org/10.1016/j.ecolind.2020.106232, 2020.

MacQueen, J.: Some methods for classification and analysis of multivariate observations, in: Proceedings of the Fifth Berkeley Symposium on Mathematical Statistics and Probability, Vol. 1: Statistics, edited by: Le Cam, L. M. and Neyman, J., University of California Press, Berkeley, CA, 281–297, https://projecteuclid.org/euclid.bsmsp/1200512992 (last access: 13 March 2026), 1967.

Marengo, J., Martinez, R., Tapia, B., Allen, T., Basantes, R., Hernandez-Espinoza, K., Alvarado, L., Baddour, O., Ransom, C., Silva, Á., Báez, J., Gomez, F., Costa, F., Avalos, G., Estella, J., and Kennedy, J.: State of the Climate in Latin America and the Caribbean 2021 (WMO-No. 1295), World Meteorological Organization, Geneva, ISBN 978-92-63-11295-8, 2022.

McDaniel, J., Kennard, D., and Fuentes, A.: Smokey the Tapir: Traditional Fire Knowledge and Fire Prevention Campaigns in Lowland Bolivia, Soc. Natur. Resour., 18, 921–931, https://doi.org/10.1080/08941920500248921, 2005.

Meinshausen, N.: Quantile Regression Forests, J. Mach. Learn. Res., 7, 983–999, 2006.

Morello, J. H. and Adámoli, J. M.: Las grandes unidades de vegetación y ambiente del Chaco argentino. Primera parte: objetivos y metodología, Serie Fitogeográfica, No. 10, Instituto Nacional de Tecnología Agropecuaria (INTA), Buenos Aires, 1–125, https://www.sidalc.net/search/Record/KOHA-OAI-FCF:1929/Description (last access: 13 March 2026), 1968.

Moreno, M. V., Laurent, P., and Mouillot, F.: Global intercomparison of functional pyrodiversity from two satellite sensors, Int. J. Remote Sens., 42, 9523–9541, https://doi.org/10.1080/01431161.2021.1999529, 2021.

Mouillot, F., Schultz, M. G., Yue, C., Cadule, P., Tansey, K., Ciais, P., and Chuvieco, E.: Ten years of global burned area products from spaceborne remote sensing – A review: Analysis of user needs and recommendations for future developments, Int. J. Appl. Earth Obs., 26, 64–79, https://doi.org/10.1016/j.jag.2013.05.014, 2014.

Mouillot, F., Chen, W., Campagnolo, M., and Ciais, P.: FRYv2.0 : a global fire patch morphology database from FireCCI51 and MCD64A1, EGU General Assembly 2023, Vienna, Austria, 24–

28 Apr 2023, EGU23-9575, https://doi.org/10.5194/egusphere-egu23-9575, 2023.

Muñoz Sabater, J.: ERA5-Land hourly data from 1950 to present, Copernicus Climate Change Service (C3S) Climate Data Store (CDS) [data set], https://doi.org/10.24381/cds.e2161bac, 2019.

Muñoz-Sabater, J., Dutra, E., Agustí-Panareda, A., Albergel, C., Arduini, G., Balsamo, G., Boussetta, S., Choulga, M., Harrigan, S., Hersbach, H., Martens, B., Miralles, D. G., Piles, M., Rodríguez-Fernández, N. J., Zsoter, E., Buontempo, C., and Thépaut, J.-N.: ERA5-Land: a state-of-the-art global reanalysis dataset for land applications, Earth Syst. Sci. Data, 13, 4349–4383, https://doi.org/10.5194/essd-13-4349-2021, 2021.

Musser, K.: Río de la Plata basin map, Wikimedia Commons, https://commons.wikimedia.org/wiki/File:Riodelaplatabasinmap.png (last access: 13 March 2026), 2010.

Myneni, R., Knyazikhin, Y., and Park, T.: MODIS/Terra Leaf Area Index/FPAR 8-Day L4 Global 500m SIN Grid V061, NASA Land Processes Distributed Active Archive Center [data set], https://doi.org/10.5067/MODIS/MOD15A2H.061, 2021a.

Myneni, R., Knyazikhin, Y., and Park, T.: MODIS/Terra+Aqua Leaf Area Index/FPAR 8-Day L4 Global 500m SIN Grid V061, NASA Land Processes Distributed Active Archive Center [data set], https://doi.org/10.5067/MODIS/MCD15A2H.061, 2021b.

Naumann, G., Podesta, G., Marengo, J., Luterbacher, J., Bavera, D., Acosta, N. J., Arias-Muñoz, C., Barbosa, P., Cammalleri, C., Cuartas, L. A., De, E. M., De, F. M., De, J. A., Escobar, C., Fioravanti, G., Giordano, L., Hrast, E. A., Hidalgo, C., Leal, D. M. O. L., Maetens, W., Magni, D., Masante, D., Mazzeschi, M., Osman, M., Rossi, L., Seluchi, M., De, L. M. S. M., Spennemann, P., Spinoni, J., Toreti, A., and Vera, C.: Extreme and long-term drought in the La Plata Basin: event evolution and impact assessment until September 2022, JRC Technical Report, Publications Office of the European Union, Luxembourg, https://doi.org/10.2760/62557, 2023.

Naval Fernández, Albornoz, J., Bellis, L. M., Baldini, C., Arcamone, J., Silvetti, L., Álvarez, M. P., and Argañaraz, J. P.: Megaincendios 2020 en Córdoba: Incidencia del fuego en áreas de valor ecológico y socioeconómico, Ecol. Austral, 33, 136–151, https://doi.org/10.25260/EA.23.33.1.0.2120, 2023.

Naval-Fernández, M. C., Elia, M., Giannico, V., Bellis, L. M., Bravo, S. J., and Argañaraz, J. P.: The Pyrogeography of the Gran Chaco's Dry Forest: A Comparison of Clustering Algorithms and the Scale of Analysis, Forests, 16, 1114, https://doi.org/10.3390/f16071114, 2025.

Nori, J., Torres, R., Lescano, J. N., Cordier, J. M., Periago, M. E., and Baldo, D.: Protected areas and spatial conservation priorities for endemic vertebrates of the Gran Chaco, one of the most threatened ecoregions of the world, Diversity and Distributions, 22, 1212–1219, https://doi.org/10.1111/ddi.12497, 2016.

Olson, D. M., Dinerstein, E., Wikramanayake, E. D., Burgess, N. D., Powell, G. V., Underwood, E. C., and Kassem, K. R.: Terrestrial Ecoregions of the World: A New Map of Life on EarthA new global map of terrestrial ecoregions provides an innovative tool for conserving biodiversity, BioScience, 51, 933–938, 2001.

Oom, D., Silva, P. C., Bistinas, I., and Pereira, J. M. C.: Highlighting Biome-Specific Sensitivity of Fire Size Distributions to Time-Gap Parameter Using a New Algorithm for Fire Event Individuation, Remote Sens., 8, 663, https://doi.org/10.3390/rs8080663, 2016.

Paritsis, J., Landesmann, J. B., Kitzberger, T., Tiribelli, F., Sasal, Y., Quintero, C., Dimarco, R. D., Barrios-García, M. N., Iglesias, A. L., Diez, J. P., Sarasola, M., and Nuñez, M. A.: Pine Plantations and Invasion Alter Fuel Structure and Potential Fire Behavior in a Patagonian Forest-Steppe Ecotone, Forests, 9, 117, https://doi.org/10.3390/f9030117, 2018.

Paudel, J.: Short-run environmental effects of COVID-19: Evidence from forest fires, World Dev., 137, 105120, https://doi.org/10.1016/j.worlddev.2020.105120, 2021.

Pausas, J. G. and Bradstock, R. A.: Fire persistence traits of plants along a productivity and disturbance gradient in mediterranean shrublands of south-east Australia, Global Ecol. Biogeogr., 16, 330–340, https://doi.org/10.1111/j.1466-8238.2006.00283.x, 2007.

Pettinari, M. L., Lizundia-Loiola, J., and Chuvieco, E.: ESA CCI ECV fire disturbance: D4. 2.1 product user guide – MODIS, version 1.1, ESA Climate Change Initiative (Fire_cci), https://climate.esa.int/en/projects/fire/key-documents/ (last access: 13 March 2026), 2021.

Pielou, E. C.: The measurement of diversity in different types of biological collections, J. Theor. Biol., 13, 131–144, https://doi.org/10.1016/0022-5193(66)90013-0, 1966.

Poulter, B., Freeborn, P., Jolly, W., and Varner, J.: COVID-19 lockdowns drive decline in active fires in southeastern United States, P. Natl. Acad. Sci. USA, 118, e2105666118, https://doi.org/10.1073/pnas.2105666118, 2021.

Redford, K. H., Taber, A., and Simonetti, J. A.: There is More to Biodiversity than the Tropical Rain Forests, Conserv. Biol., 4, 328–330, 1990.

Ruffault, J. and Mouillot, F.: How a new fire-suppression policy can abruptly reshape the fire-weather relationship, Ecosphere, 6, 199, https://doi.org/10.1890/ES15-00182.1, 2015.

Ruffault, J. and Mouillot, F.: Contribution of human and biophysical factors to the spatial distribution of forest fire ignitions and large wildfires in a French Mediterranean region, Int. J. Wildland Fire, 26, 498–508, https://doi.org/10.1071/WF16181, 2017.

Ruffault, J., Moron, V., Trigo, R. M., and Curt, T.: Objective identification of multiple large fire climatologies: an application to a Mediterranean ecosystem, Environ. Res. Lett., 11, 075006, https://doi.org/10.1088/1748-9326/11/7/075006, 2016.

Ruffault, J., Curt, T., Moron, V., Trigo, R. M., Mouillot, F., Koutsias, N., Pimont, F., Martin-StPaul, N., Barbero, R., Dupuy, J.-L., Russo, A., and Belhadj-Khedher, C.: Increased likelihood of heat-induced large wildfires in the Mediterranean Basin, Sci. Rep., 10, 13790, https://doi.org/10.1038/s41598-020-70069-z, 2020.

San Martín, R.: Fires, land use, and forest loss in the South American Chaco: understanding the links between fires, climate, ecosystems, and human activity through remote sensing, PhD Thesis, Université Paris-Saclay, NNT: 2024UPASJ034, HAL Id: tel-04885407, https://theses.hal.science/tel-04885407 (last access: 13 March 2026), 2024.

San Martín, R., Ottlé, C., and Sörensson, A.: Fires in the South American Chaco, from dry forests to wetlands: response to climate depends on land cover, Fire Ecol., 19, https://doi.org/10.1186/s42408-023-00212-4, 2023.

Saucedo, G. I. and Kurtz, D. B.: Seasonality and post fire recovery in a wetland dominated region: Insights from satellite data analysis in northern Argentina, Remote Sens-

ing Applications: Society and Environment, 37, 101480, https://doi.org/10.1016/j.rsase.2025.101480, 2025.

Schmidt, M. A. and Castilla, M.: La emergencia del fuego en un territorio hidrosocial: incendios en las provincias de Salta y Chaco, I Encuentro Territorios Hidrosociales en Disputa (ETHIS) (Chaco, 25 y 26 de agosto de 2022), Instituto de Investigaciones en Humanidades y Ciencias Sociales, 453–474, ISBN 978-987-48445-4-5, 2023.

Shannon, C. E.: A Mathematical Theory of Communication, Bell Syst. Tech. J., 27, 379–423, https://doi.org/10.1002/j.1538-7305.1948.tb01338.x, 1948.

Sugiyama, M. S., Mendoza, M., and Carpio, M. B.: Resilience and Recovery in the Dry Chaco: Ecological Knowledge Encoded in Forager Wildfire Narratives, J. Ethnobiol., 45, 76–94, https://doi.org/10.1177/02780771241303896, 2025.

Takacs, S., Schulte to Bühne, H., and Pettorelli, N.: What shapes fire size and spread in African savannahs?, Remote Sens. Ecol. Conserv., 7, 610–620, https://doi.org/10.1002/rse2.212, 2021.

Tálamo, A., Lopez De Casenave, J., Núñez-Regueiro, M., and Caziani, S. M.: Regeneración de plantas leñosas en el Chaco semiárido argentino: relación con factores bióticos y abióticos en micrositios creados por el aprovechamiento forestal, Bosque (Valdivia), 34, 13–14, https://doi.org/10.4067/S0717-92002013000100007, 2013.

Torrella, S. A. and Adámoli, J.: Situación ambiental de la ecorregión del Chaco Seco, in: La situación ambiental argentina 2005, edited by: Brown, A., Martínez Ortiz, U., Acerbi, M., and Corcuera, J., Fundación Vida Silvestre Argentina, Buenos Aires, 75–82, 2005.

Van Wagner, C. E.: Development and structure of the Canadian Forest Fire Weather Index System, Minister of Supply and Services Canada, Ottawa, 37 pp., ISBN 0-662-15198-4,, 1987.

Vidal-Riveros, C., Souza-Alonso, P., Bravo, S., Laino, R., and Ngo Bieng, M. A.: A review of wildfires effects across the Gran Chaco region, Forest Ecol. Manag., 549, 121432, https://doi.org/10.1016/j.foreco.2023.121432, 2023.

Vidal-Riveros, C., Watler Reyes, W. J., Ngo Bieng, M. A., and Souza-Alonso, P.: Assessing Fire Regimes in the Paraguayan Chaco: Implications for Ecological and Fire Management, Fire, 7, 347, https://doi.org/10.3390/fire7100347, 2024.

Vitolo, C., Di Giuseppe, F., Barnard, C., Coughlan, R., San-Miguel-Ayanz, J., Libertá, G., and Krzeminski, B.: ERA5-based global meteorological wildfire danger maps, Sci. Data, 7, 216, https://doi.org/10.1038/s41597-020-0554-z, 2020.

Wright, M. N. and Ziegler, A.: ranger: A Fast Implementation of Random Forests for High Dimensional Data in C++ and R, J. Stat. Softw., 77, 1–17, https://doi.org/10.18637/jss.v077.i01, 2017.

Yebra, M., Scortechini, G., Badi, A., Beget, M. E., Boer, M. M., Bradstock, R., Chuvieco, E., Danson, F. M., Dennison, P., Resco de Dios, V., Di Bella, C. M., Forsyth, G., Frost, P., Garcia, M., Hamdi, A., He, B., Jolly, M., Kraaij, T., Martín, M. P., Mouillot, F., Newnham, G., Nolan, R. H., Pellizzaro, G., Qi, Y., Quan, X., Riaño, D., Roberts, D., Sow, M., and Ustin, S.: Globe-LFMC, a global plant water status database for vegetation ecophysiology and wildfire applications, Sci. Data, 6, 155, https://doi.org/10.1038/s41597-019-0164-9, 2019.